scRNA-Sequencing uncovers a TCF4-dependent transcription factor network regulating commissure development

Marie-Theres Wittmann[1,2], Sayako Katada[3], Elisabeth Sock[2], Philipp Kirchner[1], Arif B. Ekici[1], Michael Wegner[2], Kinichi Nakashima[3], D. Chichung Lie[2*], André Reis[1*]

[1]Institute of Human Genetics, Universitätsklinikum Erlangen, Friedrich-Alexander-Universität Erlangen-Nürnberg (FAU), Erlangen, 91054, Germany

[2]Institute of Biochemistry, Emil Fischer Center, Friedrich-Alexander-Universität Erlangen-Nürnberg, 91054, Germany

[3]Department of Stem Cell Biology and Medicine, Graduate School of Medical Sciences, Kyushu University, Fukuoka, Japan

* Corresponding authors: chi.lie@fau.de and re.reis@uk-erlangen.de

Summary statement

Single-cell RNA Sequencing identifies interactions of TCF4 with non-bHLH transcription factors linked to neurodevelopmental and -psychiatric disease in the regulation of interhemispheric projection neuron development.

Abstract

Transcription factor 4 (TCF4) is a critical regulator of neurodevelopment and has been linked to the pathogenesis of autism, intellectual disability, and schizophrenia. As a class I bHLH transcription factor it is assumed that TCF4 exerts its neurodevelopmental functions through dimerization with proneural class II bHLH TFs. Here, we aim to identify transcription factor (TF) partners of TCF4 in the control of interhemispheric connectivity formation. Using a new bioinformatic strategy integrating TF expression levels and regulon activities from single cell RNA-

sequencing data, we find evidence that TCF4 interacts with non-bHLH TFs and modulates their transcriptional activity in *Satb2*+ intercortical projection neurons. Notably, this network comprises regulators linked to the pathogenesis of neurodevelopmental disorders, e.g. *FOXG1, SOX11* and *BRG1*. In support of the functional interaction of TCF4 with non-bHLH TFs we find that TCF4 and SOX11 biochemically interact and cooperatively control commissure formation *in vivo*, and regulate the transcription of genes implied in this process. Next to identifying new candidate interactors of TCF4 in neurodevelopment, this study illustrates how scRNA-Seq data can be leveraged to predict TFs networks in neurodevelopmental processes.

Key words: TCF4, single-cell RNA-Sequencing, Gene regulatory networks, Protein-protein interaction, SOX11, commissure development

Introduction

Transcription factor 4 (TCF4) – not to be confused with the canonical Wnt-signaling associated transcriptional regulator T-Cell factor 4 (Transcription Factor 7-Like 2, TCF7L2) - is a critical transcriptional regulator in forebrain development. Variants in *TCF4* have been associated with schizophrenia, autism and intellectual disability and *TCF4* haploinsufficiency causes the neurodevelopmental disorder Pitt-Hopkins syndrome (PTHS) (OMIM 610954) (Stefansson et al., 2009, Steinberg et al., 2011, De Rubeis et al., 2014, Zweier et al., 2007, Amiel et al., 2007).

Analyses of transgenic mice have shown that alterations of TCF4 dosage cause disruptions in neocortical neuronal migration, specification of neuronal subtypes, dendrite and synapse formation (Li et al., 2019, Page et al., 2017). Moreover, homozygous *Tcf4* loss-of-function results in deletion of all forebrain commissures in mice (Mesman et al., 2020); whereas *TCF4* haploinsufficiency in humans and in mice is associated with callosal dysgenesis (Jung et al., 2018, Zweier et al., 2007) indicating that *TCF4* is part of a conserved genetic network controlling the formation of callosal connections.

TCF4 is a class I basic Helix-Loop-Helix (bHLH) transcription factor (TF) and its transcriptional output is highly dependent on its interaction partners (Le Dreau et al., 2018). Traditionally, it is assumed that TCF4 executes its function through homodimerization or heterodimerization with proneural class II bHLH TFs such as the

Neurogenin or NeuroD family (Bertrand et al., 2002). Recent *in vitro* analysis of murine neural precursor cells raised the intriguing possibility that TCF4 has the potential to form "non-canonical" interactions, i.e. to interact with transcriptional regulators outside of the bHLH class (Moen et al., 2017). *In vivo*, cell type-specific interactors of TCF4 have not been established and it remains to be determined whether interactions of TCF4 with non-bHLH TFs are involved in the regulation of specific neurodevelopmental processes.

Here, we focused on TCF4-dependent transcriptional networks in intercortical projection neurons. First, we corroborated the recent finding that loss of *Tcf4* results in the complete agenesis of forebrain commissures in mice (Mesman et al., 2020). In subsequent analyses we used single-cell RNA sequencing (scRNA-Seq) to uncover TCF4-dependent transcriptional networks in *Satb2* expressing intercortical projection neurons. Integration of TF expression levels and regulon activities surprisingly predicted that TCF4 engages in interaction with numerous TFs outside of the bHLH class and regulates their transcriptional activity. Similar to TCF4, these interactors are often associated to neurodevelopmental disorders such as intellectual disability and autism. Reinforcing our model of TCF4-dependent transcriptional regulation by interaction, *in vitro* and *in vivo* analyses of the interaction between TCF4 and the regulator SOX11 revealed a synergistic effect of these TFs on anterior commissure (AC) and CC formation. Collectively, our study provides insight into TCF4-dependent interactions in the control of commissure formation and proposes a new strategy to harness scRNA-Seq data to predict *in vivo* transcription factor interactions in a cell type specific manner.

Results

Tcf4 knockout abolishes commissure development

Mesman and colleagues (2020) recently reported that a homozygous mutation removing the DNA binding bHLH domain from all TCF4 isoforms is associated with loss of the forebrain commissural system. Here, we analysed *Tcf4* knockout mice (*Tcf4KO*) generated by the homozygous insertion of a lacZ/neomycin cassette before exon 4 of Tcf4 (Fig. 1A). Effectiveness of the *Tcf4* knockout was assessed by western blot as there are *Tcf4* isoforms with transcriptional start sites after exon 4 (Sepp et al., 2011). Our analysis confirmed the loss of the longest TCF4 isoform (TCF4B) in the knockout; expression of a shorter isoform (TCF4A) persisted (Fig.

1B). Despite the residual TCF4 expression, *Tcf4KO* mice died shortly after birth, indicating the importance of the long TCF4 isoform during development.

In accordance with the findings of Mesman and colleagues (2020), postnatal day 0 (P0) TCF4 KO mice showed complete absence of the forebrain commissure system, i.e. CC, AC, and hippocampal commissure (Figs 1C, D, Fig. S1). Staining for the upper layer and interhemispheric projection neuron (IPN) marker SATB2 (Alcamo et al., 2008, Britanova et al., 2008) revealed a significant increase in SATB2 positive neurons (SATB2+ cells per mm^3: WT 203 ± 32; KO 270 ± 30; p - value = 0.017; Fig. 2A), which appeared to be generated at the expense of TBR1 positive (TBR1+ cells per mm^3: WT 121 ± 5; KO 101 ± 11; p - value = 0.018; Fig. 2A) but not of CTIP2 positive deep layer neurons (CTIP2+ per mm^3: WT 119 ± 21; KO 91 ± 13; p - value = 0.051; Fig. 2A). These data indicate that the commissure forming SATB2+ neurons were in principle generated in *Tcf4KO* mice. Analysis with the anterograde lipophilic tracer DiI indicated that neurons in *Tcf4KO* mice extended their axons towards the midline yet were unable to cross to the contralateral side (Fig. 1D). Staining for GAP43, a marker for the axonal growth cone verified this observation (Fig. 2B).

Development and targeting of callosal projections is dependent on the interplay between projection neurons and their environment. Hence, callosal agenesis may not only be the consequence of disrupted developmental programs in projection neurons but can also be the consequence of dysfunctional midline generation and fusion (Richards et al., 2004). Mesman and colleagues (2020) recently suggested that loss of callosal projections in their *Tcf4KO* model is caused by the loss of glial wedge glia (also known as midline glia) and failure to form a midline. We analysed our *Tcf4KO* mice at embryonic day 16.5 (E16.5), to investigate the characteristic detachment of extensions to the pial surface by GFAP-expressing glial wedge glia and the presence of CALRETININ-expressing guidepost neurons (Paul et al., 2007). Both cell types were detected at the midline in *Tcf4KO* mice and no general defect in the organization of the structure was observed (Figs 2C and D), suggesting that the midline had been properly formed. Analysis of primary cortical neurons isolated from E16.5 embryos showed that the length of the longest neurite, which will usually be specified into the axon, was significantly reduced in *Tcf4*KO neurons in comparison with WT neurons (Longest neurite length in µm: WT 226,02 ± 14,76; KO 176,59 ± 24,45; p-value = 0.012; Fig. 2E). This observation suggested that disruption of a

TCF4-dependent developmental program in neurons contributed to commissural agenesis in the present *Tcf4*KO mice.

Tcf4 knockout dysregulates genes involved in neuronal differentiation and axon guidance

To identify TCF4-dependent networks in the control of forebrain commissure formation, scRNA-Seq was conducted from E18.5 neocortices. After rigorous filtering for viable cells, 8,887 cells were analysed for the WT and 5,309 for the KO. Both the PCA and multiCCA approaches of Seurat were used for cell clustering (Butler et al., 2018, Stuart et al., 2019) and cell types were assigned using known marker expression (Figs 3A, B, Figs S2A and B). All expected major cell types were detected and WT and KO cells clustered together regardless of their genotype and of the clustering approach (Fig. 3B and Fig. S2B). Further analyses shown are based on the results of the PCA clustering; downstream analysis with the multiCCA clustering, however, yielded similar results (data not shown).

The focus of our subsequent analyses was *Satb2* expressing glutamatergic neurons as they represent IPNs normally crossing the CC and AC (Fig. 3C). To define TCF4-dependent networks in commissure forming neurons, the MAST algorithm was used to determine differentially expressed genes (DEGs) between (2,890 cells) and KO (1,328 cells) *Satb2*+ neurons (Fig. 3C and Table S1). Upregulated genes (96 genes) were associated with GO terms for ribosomes and gene expression (Fig. 3D). GO terms for downregulated genes (126 genes) included gene enrichments for neuron development (e.g. *Cd24a, Gpm6a, Neurod2* and *Ptn*), neurogenesis (e.g. *Bcl11a, Fez1, Hnrnpk* and *Id2*) as well as axon development (e.g. *Dcx, Epha5, Nfib* and *Tubb3*) (Figs 3D and E).

Analysis of unique molecular identifiers (UMIs), number of genes and the percentage of mitochondrial genes revealed that KO cells had in general a lower number of expressed genes and UMIs. We therefore limited the data to cells with less than 4000 UMIs, yielding 1057 WT and 1246 KO cells (referred to in the following as limited *Satb2* data set) and re-analysed DEG and GO term enrichment to control for potential bias introduced by differences in gene and cell number in the *Satb2* cluster. The vast majority of DEGs and GO terms remained the same indicating the biological relevance of our findings using the full *Satb2* data set (Table S2).

To ascertain that we did not introduce a bias in the analysis by defining the examined cluster only by *Satb2* expression, which appears to be affected by *Tcf4* knockout, we

also analysed the dataset using the upper (UL) and deep layer (DL) cluster that had been assigned based on known marker expression (see Figs 3A and B). The UL cluster, which is mostly consisting of IPNs, was highly comparable to the *Satb2* cluster. with 184 differentially regulated genes shared between the two cluster (*Satb2* DEG 222; UL DEG 206; Overlap 184; Figs S3 A-D and Table S3). Moreover, GO terms were highly corresponding (Table S3). For the DL cluster similar GO terms were identified, however, the underlying DEGs diverged considerably from the *Satb2* cluster (*Satb2* DEG 222; DL DEG 165; Overlap 111; Figs S3 D-H, Table S4). These results support the validity of our analysis using the *Satb2* cluster to examine *Tcf4*-dependent genetic programs in IPN development.

Collectively, these findings molecularly confirm the anatomical observation that *Tcf4* knockout affects the expression of a gene network in *Satb2* neurons/IPNs, that is involved in commissure and neuron projection development.

TCF4 modulates the activity of non-bHLH transcription factors

We next aimed to investigate the influence of TCF4 on gene regulatory networks (GRNs) using the R package SCENIC. Identified regulons were binarized to generate a high/low activity state (Fig. 4A). Re-clustering displayed a partitioning of cells between the two genotypes with only marginal overlap (Fig. 4A). Regulons were sorted into three categories: In the first, the regulon was primarily active in the WT. In the second, there was no differential activity between the genotypes, and in the third, the regulon was predominantly active in the KO. Differentially active regulons mostly fell into the first category [e.g. *Ctcf*, *Foxg1, Smarca4* (also known as *Brg1*), *Cux1*, *Pou3f3* (also known as *Brn1*), and *Sox11]* (Figs 4B and C and Table S5). As with the DEG analysis, GRN analysis was also performed with the limited *Satb2*, UL and DL datasets. In the limited *Satb2* (Table S5) and the UL dataset we found - similar to our analyses of the full *Satb2* dataset IPN specific TF-dependent regulons such as *Pou3f3* and *Cux1* being differentially active (Figs S4 A-F and Table S5). In contrast, differentially active regulons in the DL cluster represented known TF for deep layer development, e.g. *Sox5* or *Foxp2* (Figs S4 G-L and Table S5) Further analysis was therefore done with the original *Satb2* dataset.

Examination of the differentially active regulons revealed that most regulon heads were TFs. Moreover, we found an enrichment for TFs associated with intellectual disability and neurodevelopmental disorders [ID e.g. *CTCF*; neurodevelopmental disorders e.g. *FOXG1* (Fig. 4D)] (Gregor et al., 2013, Kortum et al., 2011). Surprisingly, these TFs generally did not belong to the bHLH TF family, which constitutes the canonical interaction partners of TCF4 (bHLH factors: 3.70%; Other: 96.30%) (Fig. 4E). In addition, the vast majority of regulators were not differentially expressed in the KO (DE: 6.17%; Not DE: 93.83%) (Fig. 4E), suggesting that they were not downstream targets of TCF4. A recent *in vitro* study suggested that TCF4 may interact with TFs outside the bHLH family (Moen et al., 2017). In accordance, we hypothesized that TCF4 interacts with the identified non-bHLH TFs and modulates their activity. We focused on potential interactions regulating genes involved in neurogenesis or neuron differentiation. To ensure a focus on robustly expressed regulons, the selected regulators had to be expressed in at least one quarter of the *Satb2*+ cells (Table S5). Five regulon heads [*Foxg1, Smarca4* (also known as *Brg1*), *Cux1*, *Pou3f3* (also known as *Brn1*), and *Sox11*] were selected for validation (Fig. 4C). In the context of postmitotic neurons of the cortical plate, CUX1 and POU3F3 are specifically expressed in layer II/III neurons, whereas FOXG1, SMARCA4 and SOX11 are broadly expressed during neuronal differentiation (Bergsland et al., 2006, Miyoshi and Fishell, 2012, Molyneaux et al., 2007, Deng et al., 2015). Staining of neocortical tissue at E18.5, showed that TCF4 was co-expressed with SOX11, FOXG1, SMARCA4 and POU3F3 (Fig. 4F). *In vitro* co-immunoprecipitation assays (Co-IPs) confirmed that the long TCF4 isoform has the potential to biochemically interact with all these TFs (Fig. 4G) as did proximity ligation assays in 6 day differentiated neural stem cells derived from E14.5 neocortices (Fig. S5). Collectively, these results indicate that TCF4 has the ability to biochemically interact with a wide variety of TFs and chromatin remodelers involved in neurogenesis and neuronal differentiation and suggests that these interactions are relevant for the precise execution of the developmental transcriptional program in *Satb2*+ cortical neurons.

We sought to genetically validate the functional relevance of the interaction of TCF4 and SOX11 in commissural development *in vivo* Co-IPs from E18.5 neocortex lysates confirmed the interaction of TCF4B with SOX11 *in vivo* (Fig. 4H). Notably, we did not observe a binding of SOX11 to TCF4A in the *in vivo* Co-IPs although TCF4A was detectable in the input (Fig. 4H). Next, *Tcf4* and *Sox11* haploinsufficient mice were

crossed to generate WT, *Tcf4*, *Sox11* and double *Tcf4*x*Sox11* haploinsufficient littermates. Commissural systems in P56 brains were visualized by Luxol fast blue staining. WT and *Sox11* haploinsufficient mice showed no commissural phenotype (Fig. 5A). As previously reported, *Tcf4* haploinsufficient animals had a mildly shorter CC (Jung et al., 2018). This phenotype was greatly aggravated by the additional haploinsufficiency of *Sox11* as double haploinsufficient mice showed the most severe truncation of the CC with only the rostral part of the CC remaining (agenesis of the splenium and caudal part of the body) [WT 2664 µm ± 137.64 µm; *Tcf4*Het 2320 µm ± 56.57 µm; Sox11Het 2648 µm ± 77.56 µm; Tcf4Het x Sox11Het 1816 µm ± 19.60 µm; WT vs *Tcf4*Het: p-value = 0.008; WT vs *Tcf4*Het x *Sox11*Het: p-value = 0.011; *Tcf4*Het vs *Tcf4*Het x *Sox11*Het: p-value = 0.011; *Sox11*Het vs *Tcf4*Het x *Sox11*Het: p-value = 0.011 (Fig. 5A and Fig. S6)]. Moreover, only a rudimentary AC (1 out of 5 animals) or a complete agenesis of the AC (4 out 5 animals) was observed in the double haploinsufficient mice (Fig. 5A and Fig. S6). We also performed analyses at P7 when all commissural axons have crossed the midline and started innervating the contralateral hemispheres, to distinguish whether the commissural phenotype was caused by maldevelopment or by degeneration of IPNs or their projections. Double haploinsufficient mice showed a severely truncated CC and loss of the AC at P7 (Fig. S7) indicating that the combined decrease in Sox11 and TCF4 gene dosage impaired commissural system development.

We next asked which genes may be common target genes of both TFs and thus may be involved in commissure development. Hence, we compared the predicted regulon targets of SOX11 from the GRN analysis and the list of DEGs in the *Tcf4KO*. The intersection of the datasets yielded a list of 72 genes (Fig. 5B and Table S6), which was enriched for genes linked to autism spectrum disorders and intellectual disability [ASD: e.g. *POU3F2*; ID: e.g. *DCX*; (Fig. 5C)] (Pilz et al., 1998, Martin et al., 2007). Furthermore, GO term analysis revealed an enrichment for genes associated to axonogenesis (Fig. 5D and Table S5). *Plxna2*, a gene involved in semaphorin / plexin signalling for axon guidance (Rohm et al., 2000, Mitsogiannis et al., 2017) and *Dcx*, a gene that in addition to its function in neuronal migration has been connected to neuronal morphogenesis and axon guidance (Deuel et al., 2006, Pilz et al., 1998, Yap et al., 2016, Bott et al., 2020) were selected for further investigation. Evolutionary conserved regions upstream of or at the promotor containing conserved binding sites for TCF4 and SOX11, were cloned into luciferase reporter plasmids and

transfected into HEK293T cells together with expression plasmids for TCF4 and SOX11 (Fig. 5E). SOX11 alone induced robust *Dcx* and *Plxna2* reporter activity. TCF4A or TCF4B alone only marginally induced *Plxna2* and *Dcx* activity but TCF4B strongly potentiated SOX11 induced reporter activities (Fig. 5F) supporting the general notion that Sox factors pair of with other TFs to strongly induce specific gene expression (Kamachi et al., 2000, Reiprich and Wegner, 2015). In contrast no change in activity over SOX11 alone was seen when TCF4A was co-expressed with SOX11 (Fig. 5F). To ascertain that TCF4 and SOX11 have the potential to bind to the determined regulatory regions of *Plxna2* and *Dcx* (Fig. 5E) we performed EMSAs. We were able to show the binding of both the TCF4 and the SOX11 DNA-binding domain to the regulatory regions of *Plxna2* and *Dcx* (Fig. 5G). Collectively, these data support the hypothesis that TCF4 and SOX11 can cooperate to regulate transcription of common target genes.

In summary, these findings indicate that TCF4 and SOX11 cooperate in the regulation of AC and CC formation potentially by activating expression of genes related to axonogenesis and axon guidance. These results also provide proof-of-principle that the present scRNA-Seq based strategy was suited to identify functionally relevant TCF4 interactors in a defined neuronal population.

Discussion

Here, we provide scRNA-Seq and biochemical evidence that the schizophrenia, autism and intellectual disability linked transcription factor TCF4 engages in non-canonical interactions with non-bHLH TFs to regulate the development of interhemispheric connectivity. Interestingly, a substantial fraction of TCF4 interacting transcription factors has also been associated with intellectual disability and autism raising the possibility that the TCF4-dependent regulatory network in commissure formation may be relevant for the pathogenesis of neurodevelopmental and -psychiatric disorders.

Here, we analysed *Tcf4* knockout mice generated by the homozygous insertion of a lacZ/neomycin cassette before exon 4 of *Tcf4*. This mutation disrupts the expression of longest TCF4 isoform, i.e. TCF4B, but leaves shorter isoforms such as TCF4A intact. Notably, the phenotype of our *Tcf4KO mice* is comparable with the phenotype of TCF4 homozygous KO mice harbouring a loss-of-function mutation affecting the DNA binding bHLH domain (Mesman et al., 2020, Li et al., 2019), strongly indicating that TCF4B represents the isoform that is critical for cortical layering and

commissural development. The disparity regarding the midline formation between our study and the study by Mesman and colleagues may in principle be caused by the different *Tcf4* knockout strategies and the remaining expression of shorter isoforms with DNA-binding potential. It is, however, important to keep in mind that the midline was analysed at different developmental time-points; while we performed our analyses on E16.5 – the time-point when concurrently the interhemispheric fissure is fusing, acute midline remodelling is occuring and pioneer axons are crossing into the contralateral hemisphere; Mesman and colleagues analysed the midline at P0, when interhemisphereic fissure remodelling is mostly completed (Gobius et al., 2016).

The present knockout model allows for the expression of shorter TCF4 isoforms with an intact bHLH DNA binding domain such as TCF4A. Reporter assays of genes that were predicted to be regulated by cooperation of TCF4 with SOX11 indicated i) that cooperativity with SOX11 was specific to TCF4B, and ii) that TCF4A did not impair SOX11-dependent transcriptional activity. Furthermore, *in utero* overexpression of TCF4A at E13.5, had no adverse impact on cortical layer generation (Fig. S9A). TCF4A overexpression neurons were also capable of crossing the midline (Fig. S9B). These data indicating that the cortical layering phenotype and loss of intercortical projections is caused by the loss of the longest TCF4 isoform and not by the residual expression of TCF4A. Together with the similarity in phenotypes between the present knockout mice and the TCF4 KO mice generated by disruption of the bHLH domain, these findings indicate that the remaining expression of shorter isoforms such as TCF4A neither ameliorates nor aggravates the loss-of-TCF4B phenotype.

The generation of SATB2+ neurons was not abolished by the loss of TCF4, indicating that the loss of the commissural system in *Tcf4*KO mice is not the result of a failure to generate interhemispheric projection neurons. As discussed, we could not corroborate the notion that *Tcf4KO* impairs midline formation of Mesman et al. (2020), but it is important to note that our histological analyses cannot exclude subtle defects in midline development and axon guidance cues. Our finding of defective neurite outgrowth in isolated *Tcf4KO* cortical neurons, however, indicated that *Tcf4KO* directly perturbs neurodevelopmental programs in cortical neurons.

To further understand the TCF4-dependent genetic programs in intercortical projection neurons, we performed RNA-Sequencing analysis. Previous bulk RNA-Sequencing analyses had shown that TCF4 regulates a diverse set of genes with functions in cell proliferation, neuronal differentiation, and neurotransmitter release (Li

et al., 2019, Mesman et al., 2020). Given the broad expression of TCF4 (Jung et al., 2018) and the considerable cellular diversity in the developing neocortex, available bulk RNA-Sequencing data were not ideally suited to identify cell type and or stage-specific TCF4-dependent mechanisms. We therefore used comparative single cell RNA-Sequencing analysis to zoom in onto the TCF4-dependent transcriptome in *Satb2* expressing neurons. This analysis not only allowed us to uncover potential TCF4 targets but more importantly also enabled the prediction of TCF4 interacting transcription factors in a cell type specific manner. Surprisingly, we found evidence that TCF4 interacts with a multiplicity of TFs and chromatin remodelers other than the classical interaction partners of the bHLH family.

In our new approach, prediction of functional transcription factor interaction was based on differential regulon activity. As a caveat, divergence in the activity of regulons may be a result of the unbalanced cellular coverage between genotypes during sequencing. The SCENIC algorithm, however, is considered to be relatively resistant to dropouts (Aibar et al., 2017). Furthermore, we present *in vitro* biochemical evidence for several of the predicted interactions and provide *in vivo* biochemical and genetic evidence for the cooperativity of TCF4 with the non-bHLH transcription factor SOX11 in the generation of the commissural system. We identified two potential common target genes of TCF4 and SOX11, *Dcx* and *Plxna2*, which have been shown to play important roles in axonal development and axon guidance (Rohm et al., 2000, Mitsogiannis et al., 2017, Deuel et al., 2006, Pilz et al., 1998, Yap et al., 2016, Bott et al., 2020) and are likley candidates to contribute to the observed dysgenesis of the forebrain commissures in *Tcf4*KO mice. These two genes are, however, only two exampels out of a larger network of factors involved in commissural formation which are dysregulate due to the changes in gene regulatory network activities caused by the loss of TCF4B.

Future studies should determine which domains mediate TCF4's interaction with non-bHLH transcription factors. Previous analysis had revealed the existence of multiple TCF4 isoforms (Sepp et al., 2011), with TCF4A (short isoform) and TCF4B (longest isoform) being the two main isoforms. Both, the TCF4A and TCF4B isoform were detected in protein isolates from the embryonic mouse cortex; however, only TCF4B co-immunoprecipitated with the non-bHLH transcription factor SOX11. We were also able to show that TCF4B does not impede TCF4A binding to SOX11 as TCF4A was not co-immunoprecipitated with SOX11 when using protein isolates from the

neocortex of KO mice (Fig. S10C). Moreover, the present *Tcf4KO* mouse model specifically lacks the TCF4B isoform indicating that the dysregulation of non-bHLH TF activity in these mice is dependent on TCF4B-specific domains. Collectively, our data strongly suggest that the interaction of TCF4 with non-bHLH transcription factors may be conferred by the TCF4B specific N-terminal domain.

Current evidence suggests that CC dysgenesis significantly contributes to cognitive impairment and associative dysfunction in intellectual disability, autism, and schizophrenia (Bedeschi et al., 2006, Paul et al., 2007, Rao et al., 2011, Siffredi et al., 2013, Badaruddin et al., 2007). Intriguingly, several of the predicted TCF4 interactors have been linked to neurodevelopmental disorders featuring corpus callosum abnormalities (Pringsheim et al., 2019, Filatova et al., 2019, Tzeng et al., 2014, Snijders Blok et al., 2019, Hempel et al., 2016), suggesting a pathophysiological relevance of the proposed TCF4 transcription factor network.

The present data may therefore provide a new entry point towards understanding central dysregulated networks in the pathogenesis of neurodevelopmental disorders. Additionally, the present study indicates that scRNA-Seq data can be harnessed to predict interaction partners of proteins. This powerful approach may prove valuable to infer cell type specific transcription factor networks from complex tissues thereby enabling the discovery of regulatory networks in development, physiology and disease.

Material and Methods

Contact for reagent and resource sharing

Further information and requests for resources and reagents should be directed to and will be fulfilled by the Lead Contact, André Reis (andre.reis@uk-erlangen.de).

Experimental models

All experiments were carried out in accordance with the European Communities Council Directive (86/609/EEC) and were approved by the government of Middle-Franconia. Tcf4ex4WT/lacZ mice (MGI ID: 4432303) (Jung et al., 2018) and $Sox11^{LacZ/WT}$ mice (Sock et al., 2004) were described previously.

Experiments were performed on male and female littermates between E16.5, E18.5, P0, P7 and P56. For embryonic studies, mice were bred in the afternoon and vaginal post-coitum protein plug check (“Plug check”) was performed the next morning

(defined as E0.5). Numbers of animals used in each experiment are indicated in the figure legends.

Genotyping of the mice was done using the following primers:

Tcf4ex4WT/lacZ	fwd Mut	TCGTGGTATCGTTATGCGCC
	Fwd WT	CCGATGACAGTGATGATGGT
	rev	AAGTTAAGCTGAAGTAAATACCCACA
	lacZ fwd	ATCACGACGCGCTGTATC
	lacZ rev	ACATCGGGCAAATAATATCG
$Sox11^{LacZ/WT}$	fwd	GCCCGCGCAGGAGACCGAGC
	Rev	CTTGTAGTCGGGGTAGTCAGCC
	lacZ	CGCTCAGGTCAAATTCAGAC

Tissue preparation and dissection

Timed pregnant mice were killed by cervical dislocation. For the E16.5, E18.5 and P0 time points, brains were dissected and fixed overnight in 4% PFA. Tails were used for genotyping. After fixation tissue was transferred to 30% sucrose in 0.1 M phosphate buffer overnight for dehydration. Embryonic tissues were embedded in freezing media (Leica Biosystems, Richmond) and stored at −80°C. P7 mice and adult mice (P56) were killed using CO_2 and transcardially perfused with PBS for 2 min (20 ml/min) followed by fixation with 4% paraformaldehyde (PFA) in PBS, pH 7.4, for 5 min. The brains were post-fixed overnight in 4% PFA at 4°C followed by dehydration at 4°C in 30% sucrose in 0.1 M phosphate buffer.

Histology

Embryonic tissue was cut serially in 10 µm thin sections with a cryotom (Leica Microsystems, Wetzlar). Sections were transferred on laminated object slides, dried for 2 h at room temperature (RT) and stored at −80°C. Slides were washed once for 5 min with 1x PBS. For antigen retrieval, sections were treated with 10 mM citrate buffer (pH 6) for 11 min at 720 watt in the microwave. Half of the citrate buffer was replaced by water and the sections were incubated for another 30 min. Slides were washed once in 1x PBS and then incubated in 4% PFA for 10 min followed by two more washing steps in 1x PBS. Tissue was permeabilized for 10 min in 0.3% Triton-X/PBS and blocked with blocking solution (10% Donkey serum, 3% BSA and 0.1% Tween20 in PBS) for 1 h in a wet chamber at RT. Sections were incubated with primary antibodies [rb BRN1 (kind gift of Elisabeth Sock; Schreiber et al., 1997)

1:500); rb BRG1 (Santa Cruz, sc10768) 1:100; rb CALRETININ (Swant 7699/4) 1:500; rt CTIP2 (Abcam, 18465) 1:500; rb FOXG1 (Abcam, ab18259) 1:500; rb GAP43 (Abcam, ab5220) 1:500; ch GFAP (Abcam, ab4674) 1:500; ms SATB2 (Santa Cruz, sc-81376), 1:500; rat anti-SOX11 (kind gift from Johannes Glöckner) 1:500; rb TBR1 (Abcam, ab31940) 1:500; ms TCF4 (Santa Cruz, sc393407) 1:100] diluted in blocking solution at 4°C overnight. Slides were washed three times for 5 min with 1x 0.1% Tween/PBS, incubated with secondary antibodies diluted in blocking solution for 2 h at RT, and washed three times with 1x PBS. Nuclei were stained with DAPI (500 pg/ml in 1x PBS) for 10 min. After additional washing with 1x PBS for 5 min, slides were mounted with 60 µl Mowiol (Sigma Aldrich Chemie GmbH Munich, Germany) and stored at 4 C.

Cell counting

Cell counting was done blind to avoid bias. Numbers were randomly assigned to slides before imaging. Genotypes were only revealed for statistical analysis. All images were taken with the pial surface at the upper edge of the picture and the ventricular surface at the lower edge. Cells were counted using ImageJ software and reported as the density of marker positive cells per mm^3 of cortical area counted. For each animal one rostral and caudal section of the neocortex was counted.

Lipophilic Tracer Analysis

For the lipophilic tracer experiment P0 brains were dissected and washed once in 1x PBS. 1 µl of DiI dilution [DiIC18(3), Invitrogen, Eugene, Orgeon] was pipetted on one hemisphere and the brain fixed in 4% PFA. After six weeks the tissue was transferred to 30% sucrose in 0.1 M phosphate buffer overnight and subsequently treated as described in the histology section and only counterstained with DAPI.

Primary cortical neuron culture and neurite measurement

To generated primary cortical neuron cultures, timed pregnant mice were killed by cervical dislocation at E16.5 and the neocortices of single embryos were dissected under a binocular and immediately transferred to ice cold HBSS (GIBCO). Tails were used for genotyping. After removal of HBSS the tissue was incubated in 2 ml dissociation medium [HBSS (GIBCO), 0.01% Papain (Sigma-Aldrich), 0.1% Dispase

II (Roche), 0.01% DNAse I (Roche) and 12,4 mM $MgSO_4$) for 10 min at 37°C after which the solution was then gently triturated ten times with a glas pipette. This step was repeated two more times. Cells were strained with a 70 µm strainer, which was washed with 1 ml of NBA-Mix [Neurobasal Medium (GIBCO), 0.2 mM GlutaMax™ (GIBCO), 1xNeurobrew-21 (MACS Miltenyi Biotec), 0.1M NaPyr (GIBCO) and 0.1M Anti-Anti (GIBCO)]. The solution was centrifuged for 5 min at 120 g and then washed with 1 ml NBA-Mix and centrifuged again. This step was repeated another time. 200000 cells were seeded on PDL/laminin coated coverslips in a 24 well plates. Cells were fixed after 3 days in vitro and stained with rb TUBB3 (Abcam, 18207) 1:500, ms SATB2 (Santa Cruz, sc-81376) 1:500, rt CTIP2 (Abcam, 18465) 1:500 and DAPI. Single neurons, which did not contact other neurons in the vicinity and only expressed SATB2, but not CTIP2, were imaged for analysis to ensure that only intercortical projection neurons are compared. 20 cells per animal were analysed. Longest neurite lengths were measured from the soma to the tip of the longest neurite using the Simple neurite tracer tool of Fiji (Longair et al., 2011).

Luxol fast blue staining

Brains were serially cut into 40 µm sections. Free floating sections were washed two times with 1x PBS, mounted on coated adhesive glass slides and dried for at least 2 h at RT. The glass slides were incubated in luxol fast blue solution (Polyscience, Hirschberg an der Bergstraße) at 57°C overnight and washed one time in 95% ethanol and one time in distilled water. The staining was differentiated in lithium carbonate solution for 3 min followed by incubation in 70% ethanol till white and grey matter was distinguishable. The nuclei were stained with Mayer´s hemalun solution for 30 sec and rinsed with tap water. Slides were mounted with 60 µl Mowiol and stored at 4°C. To quantify the length of the corpus callosum, the slices were counted from the first slices to last slices showing a corpus callosum.

Imaging

For overview images, cell counting and neurite length measurement, fluorescence signal was detected with an AF6000 Modular Systems Leica fluorescent microscope and documented with a SPOT-CCD camera and the Leica software LAS AF (Version 2.6.0.7266; Leica Microsystems, Wetzlar Germany). For the analysis of the Luxol fast blue staining, images were obtained with a Zeiss MN Imager and x 2.5 objective lens. For co-expression analysis, fluorescence signal was detected using a Zeiss LSM 780

confocal microscope with four lasers (405, 488, 550, and 633 nm) and × 40 objective lens. Images were processed using ImageJ.

Co-immunoprecipitation

For *in vitro* Co-immunoprecipitation (Co-IP) HEK 293T cells (ATCC, Wesel, Germany; CRL-3216) were seeded in 10 cm dishes in DMEM supplemented with 10% of fetal bovine serum and 5 ml penicillin/Streptomycin. At a confluency of 70-90% cells were transfected using JETPEI (Polyplus transfection, 101-10 N) with equal amounts of the expression vectors (7.5 µg/10 cm dish) of CAG-TCF4-IRES-GFP and the predicted interaction partners [pCMV5 rBrn1(Schreiber et al., 1997); pBJ5-hBRG1(pBJ5 hBRG1 was a gift from Jerry Crabtree; Addgene plasmid # 17873)(Khavari et al., 1993); pXJ42-p200 CUX1 (pXJ42-p200 CUX1 was a gift from Alain Nepveu; Addgene; plasmid # 100813)(Wilson et al., 2009); CAG-*Foxg1*-IRES-RFP; CAG-*Sox11*-IRES-GFP (Balta et al., 2018)) according to the manufacturer instruction. After 48 h, three 10 cm dishes were harvested in 1 ml Buffer A [10 mM Hepes, pH 7.9, 10 mM KCl, 0.1 mM EDTA, pH 8.0, 0.1 mM EGTA, pH 8.0, protease inhibitor EDTA free cocktail (Roche PVT GmbH Waiblingen, Germany) and Phosphatase Inhibitors Cocktail (Sigma Aldrich Chemie GmbH Munich, Germany)]. After addition of 100 µl of 10% NP-40 and 84 µl of 5 M NaCl the solution was vortexed followed by 15 min of incubation on a rotating wheel at 4°C. The homogenates were centrifuged at 14000xg for 3 min. The supernatant was used directly for the Co-IP by mixing 300 µl with 1.2 ml of TEN-Buffer [10 mM Tris, pH 7.4, 0.05 mM EDTA, 50 mM NaCl, 0.25% 10%NP40, protease inhibitor EDTA free cocktail and Phosphatase Inhibitors Cocktail] and 2 µl of ms TCF4-antibody (Santa Cruz, sc393407), 2 µl of ms BrdU-antibody (BD Bioscience, B44) (Control for unspecific binding to mouse antibodies), or nothing to control for unspecific binding to the Beads. An appropriate amount of the supernatant was kept as Input. Probes were incubated on a rotating wheel at 4°C overnight. 30 µl of Protein A Agarose Beads, Fast Flow (Millipore-Merck, Darmstadt) in TEN-Buffer (1:1) were added and the samples were rotated for another 3 h at 4°C. Samples were centrifuged for 5 min at 1200xg and the supernatant was discarded. Beads were washed three times with 500 µl of TEN-Buffer and frozen at -80°C. For Western Blot analysis 30 µl of 3xLaemmli buffer was added to samples and incubated at 95°C for 5 min. 25 µl of the samples were loaded on 10% SDS gels.

For *in vivo* Co-IP, neocortices of E18.5 WT embryos were dissected. Two cortices were homogenized in 1 ml of Buffer A. Samples were treated as described above. Antibodies used were rb SOX11-antibody (Abcam, ab134107) and rb Cre-antibody (Abcam, ab110465). For Western Blot analysis 50 µl of 3x Laemmli buffer was added to the beads and incubated by 95°C for 5 min. 20 µl of the samples were loaded on 10% SDS gels or 4-12% Bis-Tris gels.

Western Blot

Protein extracts from E18.5 WT or KO cortices were obtained by homogenizing the tissue in RIPA buffer [50 mM Tris-HCl, pH 8.0, 150 mM NaCl, 1% Nonidet P-40, 0.5% Na-deoxycholate, 0.1% SDS, 2 mM EDTA, protease inhibitor EDTA free cocktail and Phosphatase Inhibitors Cocktail] followed by incubation for 30 min on ice. The post-nuclear supernatant of the lysate was obtained by centrifugation at 2000xg for 10 min at 4°C. Protein content was measured using the Pierce BCA protein assay (Thermo Scientific, Warrington, UK). 30 µg of protein were loaded on a 10% SDS-PAGE gel. Gels underwent wet transfer onto a nitrocellulose membrane. Membranes were blocked in PBS with 0.1% Tween 20 (PBS-T). Incubation with primary antibodies diluted in 5% BSA in PBS-T was performed overnight at 4°C and was followed by three times washing with PBS-T. Secondary antibodies were diluted in PBST and incubated with the membranes for 1 h at RT followed by washing with PBS-T. Membranes were treated with Clarity Western Enhanced Chemiluminescence Substrate (Bio-Rad) and visualized with Fusion-SL (PeqLab). Images were processed via Fusion (PeqLab).

Luciferase Assay

The ECR from the *Plxna2 gene* had the following positions in Mm10: chr1:194607209-194608066 (Fig. S9). The ECR was obtained by PCR from WT mouse DNA and inserted into the pTATA luciferase reporter plasmid between XhoI and SacI sites in front of a β-globin minimal promoter (the plasmid was based on Kuhlbrodt et al. (1998)). The hDCX-Promotor plasmid has been described before in Karl et al. (2005). In short, the 3509 bp regulatory region (Fig. S9) of the *DCX* promotor was subcloned into a vector (pGl3-Basic) containing the gene for firefly luciferase (Promega, Madison, WI, USA).

HEK cells were seeded in a density of 80.000 cells per well in a 24 well plate and transfected the next day. 300 ng of CAG-GFP-based expression vectors in total

(CAG-GFP; CAG-*Sox11*-IRES-GFP (Balta et al., 2018); CAG-TCF4A-IRES-GFP, CAG-TCF4B-IRES-GFP, 100 ng of luciferase reporter (hDCX-pGL3 (Karl et al., 2005) or pTataLuc-Plxna2) and 10 ng of Renilla expression plasmid per well were transfected using JETPEI (Polyplus transfection, 101-10 N) according to the manufacturers' instruction. Three independent biological replicates were performed, with three technical replicates for each condition per biological replicate. After 48 h Luciferase assay was performed according to manufacturers' instruction using the Dual-Luciferase Reporter Assay System Kit (Promega).

Electrophoretic mobility shift assays (EMSA)

Protein extracts were obtained by transfecting HEK293 cells with JETPEI (Polyplus transfection, 101-10 N) using 5 µg expression plasmid per 10 cm plate, and harvested 48 h post-transfection with Buffer A as described in the Co-IP section. pCMV5, pCMV5-Sox11-HMG (coding for amino acids 38–126 of SOX11) and pCMV5-TCF4-bHLH-T7 (coding for amino acids 491-617 of the TCF4B isoform) were used for transfection.

Electrophoretic mobility shift assays (EMSA) were performed in the presence of 1 µg poly-dGdC (SOX11) or 0.3 µg sheared salmon sperm DNA (100–400 bp) (TCF4) as unspecific competitor using 32P-labeled 25-52 bp long double-stranded oligonucleotides and HEK293 whole-cell extracts (Kuhlbrodt et al., 1998). Oligonucleotides contained putative Sox11-binding sites or E-boxes identified in the ECRs (see Fig. 5E).

Single-cell RNA sequencing and analysis

Single-Cell Isolation of E18.5 cortex tissue

Neocortices of E18.5 embryos were dissected, and each cortex was incubated in 150 µl of Ovomucoid-Mix [1.15 mg/ml Trypsin-Inhibitor (Sigma Aldrich Chemie GmbH Munich, Germany), 0.53 mg/ml BSA, 400 ng/ml DNase I Type IV (Roche PVT GmbH Waiblingen, Germany) in L15 medium (Gibco)] and cut into small pieces. After addition of 150 µl of Papain-Mix (30 U/ml Papain (Sigma Aldrich Chemie GmbH Munich, Germany), 0.24 mg/ml Cysteine (Sigma Aldrich Chemie GmbH Munich, Germany), 40 µg/ml DNase I Type IV (Roche PVT GmbH Waiblingen, Germany)) samples were incubated for 15-20 min at 37°C. 300 µl of Ovomucoid-Mix was added followed by a 5 min incubation at RT. The tissue was triturated with fire-polished glass pipettes, transferred to 10 ml of L15 medium and centrifuged for 5 min at 90xg.

About 9.5 ml of the supernatant was discarded. Cells were resuspended in the remaining media and strained (Mesh size: 40 µm) to remove clumps. Cell density was determined using a Neubauer chamber. Libraries were prepared using the Chromium Controller and the Chromium Single Cell 3' Reagent Kit v2 (10X Genomics, Pleasanton, CA) according to manufacturers' instructions. Single cell suspensions were diluted in nuclease-free water according to manufacturer instructions to obtain a targeted cell count of 5000. Libraries were sequenced as described previously (Lukassen et al., 2018).

Data Processing for scRNA-Seq Analysis Using Cell Ranger and Seurat

The reads were de-multiplexed using Cell Ranger (version 2.1.1, 10X Genomics). mkfastq and read quality was assessed by FastQC (version 0.11.8, Babraham bioinformatics). For mapping the reads to the mm10 genome (10X Reference 2.1.0, GRCm38, Ensembl 84) and to identify single cells the standard Cell Ranger workflow was used. Common quality control measures for scRNA-Seq (gene count per cell, UMI count per cell, percent of mitochondrial transcripts) were calculated using the Seurat R package (version 2.3.4) (Butler et al., 2018, Stuart et al., 2019). The analyses were performed for genotypes and for each mouse individually. Quality control thresholds were set to 1,000-5,000 genes per cells, 1800-10000 UMIs and <6% of mitochondrial transcripts. Only samples with more than 500 cells after filtering were used to ensure a complete reproduction of cell diversity in the neocortex. Therefore, 2 samples for the WT and 2 samples for the KO were removed. 3 samples for WT and 2 samples for KO were used for further analysis. We had to exclude one WT animal that displayed lower *Tcf4* expression than the KO and excluded cells that displayed a high background transcript expression of blood related genes such as *Hbb-a1*.

scRNA-Seq clustering and differential gene expression analysis using Seurat

Clustering of the cells was performed using the Seurat packages for R following the vignettes of the authors (Guided tutorial --- 2700 PBMCs for PCA approach or Stimulated and Control PBMCs for multiCCA approach, version 2.3.4) (Butler et al., 2018, Stuart et al., 2019). Cluster identity was defined using known marker expression. To extract *Satb2* expressing glutamatergic cells, the data was subset by accepting only cells belonging to the intermediate progenitor, newborn neuron, deep layer and upper layer clusters with counts for *Satb2* above 0. Differentially expressed

genes between the two genotypes were determined using the MAST algorithm as implemented in Seurat with nUMIs as confounding variable to adjust for cellular detection rate (Finak et al., 2015). GO-terms were identified with the Panther online tool (GO- Slim biological process and GO biological process complete) (http://www.pantherdb.org) (Mi et al., 2019).

Gene regulatory network analysis by SCENIC

Assessment of gene regulatory networks (GRNs) was performed using the R package SCENIC (version 1.1.01) (Aibar et al., 2017). Only genes expressed in at least three cells were considered for analysis which was performed according to the package vignettes. After gene regulatory networks were defined, the networks were binarized. To that end a threshold was set at the mean of the area under the curve which separated cells into cells with low and high activity. Cells clustered apart according to their genotype and differentially active GRNs were identified by. Only genes associated with the GO terms neurogenesis/neuron differentiation and with at least an expression in 1/4 of the cells in the *Satb2* cluster were chosen for validation of the hypothesis that TCF4 interacts with the regulators. Common targets of TCF4 and SOX11 were found by intersecting the list of DEGs from the *Satb2* cluster with the predicted targets of the Sox11 regulon. Enrichment for disease association in the list of differentially active regulons or of the common targets of TCF4 and Sox11 was determined using DOSE (Yu et al., 2015).

Statistical analysis

The shapiro-wilks test in R was used to determine normal distribution of all data. If normality can be assumed the two-tailed student´s t-test of the ggplot2 implementation of R was used to determine statistical significance. Otherwise, a Mann-Whitney-U test was performed using the ggplot2 implementation of R.

To determine whether differences in luciferase activities (Fig. 4E) were statistically significant, a two-tailed student´s t-test was performed using the ggplot2 implementation of R.

Data is depicted as mean ± SD. (*, P ≤0.05; **, P ≤0.01, ***, P ≤0.001).

Data availability

The accession number for the single-cell RNA Sequencing of E18.5 neocortices is GEO: GSE147247.

Acknowledgments

We thank Sven Falk, Silvia Cappello and all members of the Institutes of Human Genetics and Biochemistry for helpful discussions. We thank Tõnis Timmusk for the kind gift of pcDNA3-plasmid for TCF4A and TCF4B isoforms.

Declaration of Interests

The authors declare no competing interests.

Author contributions

Conceptualization, M.-T.W., D.C.L., A.R; Investigation, M.-T.W., S.K., E.S., P.K., A.B.E., Formal analysis, M.-T.W., S.K., E.S., P.K., A.B.E., M.W., K.N., D.C.L., A.R; Resources and Funding acquisition, D.C.L., A.R; Reagents, E.S., M.W., K.N.; Writing-Original draft, M.-T.W., D.C.L., A.R.; Writing-Review and Editing, M.-T.W., D.C.L., A.R.; Supervision: D.C.L., A.R.

Funding

This work was supported by the Deutsche Forschungsgemeinschaft (DFG, German Research Foundation) [Grant numbers 270949263/ GRK2162 and LI 858/ 9-1], by the Interdisciplinary Centre for Clinical Research Erlangen [Grant number E16 to D.C.L. and A.R.], and Bavarian Research Association: Interaction of human brain cells (ForInter) funded by Bavarian State Ministry of Science and the Arts to D.C.L.. Microscopy/Image analysis was performed with support from DFG grant INST 410/45-1 FUGG.

M.T.W. is member of the research training group 2162 “Neurodevelopment and Vulnerability of the Central Nervous System” of the Deutsche Forschungsgemeinschaft (DFG GRK2162/1)

References

AIBAR, S., GONZALEZ-BLAS, C. B., MOERMAN, T., HUYNH-THU, V. A., IMRICHOVA, H., HULSELMANS, G., RAMBOW, F., MARINE, J. C., GEURTS, P., AERTS, J., VAN DEN OORD, J., ATAK, Z. K., WOUTERS, J. & AERTS, S. 2017. SCENIC: single-cell regulatory network inference and clustering. *Nat Methods,* 14**,** 1083-1086.

ALCAMO, E. A., CHIRIVELLA, L., DAUTZENBERG, M., DOBREVA, G., FARINAS, I., GROSSCHEDL, R. & MCCONNELL, S. K. 2008. Satb2 regulates callosal projection neuron identity in the developing cerebral cortex. *Neuron,* 57**,** 364-77.

AMIEL, J., RIO, M., DE PONTUAL, L., REDON, R., MALAN, V., BODDAERT, N., PLOUIN, P., CARTER, N. P., LYONNET, S., MUNNICH, A. & COLLEAUX, L. 2007. Mutations in TCF4, encoding a class I basic helix-loop-helix transcription factor, are responsible for Pitt-Hopkins syndrome, a severe epileptic encephalopathy associated with autonomic dysfunction. *Am J Hum Genet,* 80**,** 988-93.

BADARUDDIN, D. H., ANDREWS, G. L., BOLTE, S., SCHILMOELLER, K. J., SCHILMOELLER, G., PAUL, L. K. & BROWN, W. S. 2007. Social and behavioral problems of children with agenesis of the corpus callosum. *Child Psychiatry Hum Dev,* 38**,** 287-302.

BALTA, E. A., SCHAFFNER, I., WITTMANN, M. T., SOCK, E., VON ZWEYDORF, F., VON WITTGENSTEIN, J., STEIB, K., HEIM, B., KREMMER, E., HABERLE, B. M., UEFFING, M., LIE, D. C. & GLOECKNER, C. J. 2018. Phosphorylation of the neurogenic transcription factor SOX11 on serine 133 modulates neuronal morphogenesis. *Sci Rep,* 8**,** 16196.

BEDESCHI, M. F., BONAGLIA, M. C., GRASSO, R., PELLEGRI, A., GARGHENTINO, R. R., BATTAGLIA, M. A., PANARISI, A. M., DI ROCCO, M., BALOTTIN, U., BRESOLIN, N., BASSI, M. T. & BORGATTI, R. 2006. Agenesis of the corpus callosum: clinical and genetic study in 63 young patients. *Pediatr Neurol,* 34**,** 186-93.

BERGSLAND, M., WERME, M., MALEWICZ, M., PERLMANN, T. & MUHR, J. 2006. The establishment of neuronal properties is controlled by Sox4 and Sox11. *Genes Dev,* 20**,** 3475-86.

BERTRAND, N., CASTRO, D. S. & GUILLEMOT, F. 2002. Proneural genes and the specification of neural cell types. *Nat Rev Neurosci,* 3**,** 517-30.

BOTT, C. J., MCMAHON, L. P., KEIL, J. M., YAP, C. C., KWAN, K. Y. & WINCKLER, B. 2020. Nestin Selectively Facilitates the Phosphorylation of the Lissencephaly-Linked Protein Doublecortin (DCX) by cdk5/p35 to Regulate Growth Cone Morphology and Sema3a Sensitivity in Developing Neurons. *J Neurosci,* 40**,** 3720-3740.

BRITANOVA, O., DE JUAN ROMERO, C., CHEUNG, A., KWAN, K. Y., SCHWARK, M., GYORGY, A., VOGEL, T., AKOPOV, S., MITKOVSKI, M., AGOSTON, D., SESTAN, N., MOLNAR, Z. & TARABYKIN, V. 2008. Satb2 is a postmitotic determinant for upper-layer neuron specification in the neocortex. *Neuron,* 57**,** 378-92.

BUTLER, A., HOFFMAN, P., SMIBERT, P., PAPALEXI, E. & SATIJA, R. 2018. Integrating single-cell transcriptomic data across different conditions, technologies, and species. *Nat Biotechnol*, 36, 411–420.

DE RUBEIS, S., HE, X., GOLDBERG, A. P., POULTNEY, C. S., SAMOCHA, K., CICEK, A. E., KOU, Y., LIU, L., FROMER, M., WALKER, S., SINGH, T., KLEI, L., KOSMICKI, J., SHIH-CHEN, F., ALEKSIC, B., BISCALDI, M., BOLTON, P. F., BROWNFELD, J. M., CAI, J., CAMPBELL, N. G., CARRACEDO, A., CHAHROUR, M. H., CHIOCCHETTI, A. G., COON, H., CRAWFORD, E. L., CURRAN, S. R., DAWSON, G., DUKETIS, E., FERNANDEZ, B. A., GALLAGHER, L., GELLER, E., GUTER, S. J., HILL, R. S., IONITA-LAZA, J., JIMENZ GONZALEZ, P., KILPINEN, H., KLAUCK, S. M., KOLEVZON, A., LEE, I., LEI, I., LEI, J., LEHTIMAKI, T., LIN, C. F., MA'AYAN, A., MARSHALL, C. R., MCINNES, A. L., NEALE, B., OWEN, M. J., OZAKI, N., PARELLADA, M., PARR, J. R., PURCELL, S., PUURA, K., RAJAGOPALAN, D., REHNSTROM, K., REICHENBERG, A., SABO, A., SACHSE, M., SANDERS, S. J., SCHAFER, C., SCHULTE-RUTHER, M., SKUSE, D., STEVENS, C., SZATMARI, P., TAMMIMIES, K., VALLADARES, O., VORAN, A., LI-SAN, W., WEISS, L. A., WILLSEY, A. J., YU, T. W., YUEN, R. K., STUDY, D. D. D., HOMOZYGOSITY MAPPING COLLABORATIVE FOR, A., CONSORTIUM, U. K., COOK, E. H., FREITAG, C. M., GILL, M., HULTMAN, C. M., LEHNER, T., PALOTIE, A., SCHELLENBERG, G. D., SKLAR, P., STATE, M. W., SUTCLIFFE, J. S., WALSH, C. A., SCHERER, S. W., ZWICK, M. E., BARETT, J. C.,

CUTLER, D. J., ROEDER, K., DEVLIN, B., DALY, M. J. & BUXBAUM, J. D. 2014. Synaptic, transcriptional and chromatin genes disrupted in autism. *Nature,* 515**,** 209-15.

DENG, L., LI, G., RAO, B. & LI, H. 2015. Central nervous system-specific knockout of Brg1 causes growth retardation and neuronal degeneration. *Brain Research,* 1622**,** 186-195.

DEUEL, T. A., LIU, J. S., CORBO, J. C., YOO, S. Y., RORKE-ADAMS, L. B. & WALSH, C. A. 2006. Genetic interactions between doublecortin and doublecortin-like kinase in neuronal migration and axon outgrowth. *Neuron,* 49**,** 41-53.

FILATOVA, A., REY, L. K., LECHLER, M. B., SCHAPER, J., HEMPEL, M., POSMYK, R., SZCZALUBA, K., SANTEN, G. W. E., WIECZOREK, D. & NUBER, U. A. 2019. Mutations in SMARCB1 and in other Coffin-Siris syndrome genes lead to various brain midline defects. *Nat Commun,* 10**,** 2966.

FINAK, G., MCDAVID, A., YAJIMA, M., DENG, J., GERSUK, V., SHALEK, A. K., SLICHTER, C. K., MILLER, H. W., MCELRATH, M. J., PRLIC, M., LINSLEY, P. S. & GOTTARDO, R. 2015. MAST: a flexible statistical framework for assessing transcriptional changes and characterizing heterogeneity in single-cell RNA sequencing data. *Genome Biol,* 16**,** 278.

GOBIUS, I., MORCOM, L., SUAREZ, R., BUNT, J., BUKSHPUN, P., REARDON, W., DOBYNS, W. B., RUBENSTEIN, J. L., BARKOVICH, A. J., SHERR, E. H. & RICHARDS, L. J. 2016. Astroglial-Mediated Remodeling of the Interhemispheric Midline Is Required for the Formation of the Corpus Callosum. *Cell Rep,* 17**,** 735-747.

GREGOR, A., OTI, M., KOUWENHOVEN, E. N., HOYER, J., STICHT, H., EKICI, A. B., KJAERGAARD, S., RAUCH, A., STUNNENBERG, H. G., UEBE, S., VASILEIOU, G., REIS, A., ZHOU, H. & ZWEIER, C. 2013. De novo mutations in the genome organizer CTCF cause intellectual disability. *Am J Hum Genet,* 93**,** 124-31.

HEMPEL, A., PAGNAMENTA, A. T., BLYTH, M., MANSOUR, S., MCCONNELL, V., KOU, I., IKEGAWA, S., TSURUSAKI, Y., MATSUMOTO, N., LO-CASTRO, A., PLESSIS, G., ALBRECHT, B., BATTAGLIA, A., TAYLOR, J. C., HOWARD, M. F., KEAYS, D., SOHAL, A. S., COLLABORATION, D. D. D., KUHL, S. J., KINI, U. & MCNEILL, A. 2016. Deletions and de novo mutations of SOX11 are associated with a neurodevelopmental disorder with features of Coffin-Siris syndrome. *J Med Genet,* 53**,** 152-62.

JUNG, M., HABERLE, B. M., TSCHAIKOWSKY, T., WITTMANN, M. T., BALTA, E. A., STADLER, V. C., ZWEIER, C., DORFLER, A., GLOECKNER, C. J. & LIE, D. C. 2018. Analysis of the expression pattern of the schizophrenia-risk and intellectual disability gene TCF4 in the developing and adult brain suggests a role in development and plasticity of cortical and hippocampal neurons. *Mol Autism,* 9**,** 20.

KAMACHI, Y., UCHIKAWA, M. & KONDOH, H. 2000. Pairing SOX off: with partners in the regulation of embryonic development. *Trends Genet,* 16**,** 182-7.

KARL, C., COUILLARD-DESPRES, S., PRANG, P., MUNDING, M., KILB, W., BRIGADSKI, T., PLOTZ, S., MAGES, W., LUHMANN, H., WINKLER, J., BOGDAHN, U. & AIGNER, L. 2005. Neuronal precursor-specific activity of a human doublecortin regulatory sequence. *J Neurochem,* 92**,** 264-82.

KHAVARI, P. A., PETERSON, C. L., TAMKUN, J. W., MENDEL, D. B. & CRABTREE, G. R. 1993. BRG1 contains a conserved domain of the SWI2/SNF2 family necessary for normal mitotic growth and transcription. *Nature,* 366**,** 170-4.

KORTUM, F., DAS, S., FLINDT, M., MORRIS-ROSENDAHL, D. J., STEFANOVA, I., GOLDSTEIN, A., HORN, D., KLOPOCKI, E., KLUGER, G., MARTIN, P., RAUCH, A., ROUMER, A., SAITTA, S., WALSH, L. E., WIECZOREK, D., UYANIK, G., KUTSCHE, K. & DOBYNS, W. B. 2011. The core FOXG1 syndrome phenotype consists of postnatal microcephaly, severe mental retardation, absent language, dyskinesia, and corpus callosum hypogenesis. *J Med Genet,* 48**,** 396-406.

KUHLBRODT, K., HERBARTH, B., SOCK, E., HERMANS-BORGMEYER, I. & WEGNER, M. 1998. Sox10, a novel transcriptional modulator in glial cells. *J Neurosci,* 18**,** 237-50.

LE DREAU, G., ESCALONA, R., FUEYO, R., HERRERA, A., MARTINEZ, J. D., USIETO, S., MENENDEZ, A., PONS, S., MARTINEZ-BALBAS, M. A. & MARTI, E. 2018. E proteins sharpen neurogenesis by modulating proneural bHLH transcription factors' activity in an E-box-dependent manner. *Elife,* 7:e37267.

LI, H., ZHU, Y., MOROZOV, Y. M., CHEN, X., PAGE, S. C., RANNALS, M. D., MAHER, B. J. & RAKIC, P. 2019. Disruption of TCF4 regulatory networks leads to abnormal cortical development and mental disabilities. *Mol Psychiatry*, 24, 1235–1246.

LONGAIR, M. H., BAKER, D. A. & ARMSTRONG, J. D. 2011. Simple Neurite Tracer: open source software for reconstruction, visualization and analysis of neuronal processes. *Bioinformatics,* 27**,** 2453-4.

LUKASSEN, S., BOSCH, E., EKICI, A. B. & WINTERPACHT, A. 2018. Single-cell RNA sequencing of adult mouse testes. *Sci Data,* 5**,** 180192.

MARTIN, C. L., DUVALL, J. A., ILKIN, Y., SIMON, J. S., ARREAZA, M. G., WILKES, K., ALVAREZ-RETUERTO, A., WHICHELLO, A., POWELL, C. M., RAO, K., COOK, E. & GESCHWIND, D. H. 2007. Cytogenetic and molecular characterization of A2BP1/FOX1 as a candidate gene for autism. *Am J Med Genet B Neuropsychiatr Genet,* 144B**,** 869-76.

MESMAN, S., BAKKER, R. & SMIDT, M. P. 2020. Tcf4 encodes correct brain development during embryogenesis. *Mol Cell Neurosci***,** 103502.

MI, H., MURUGANUJAN, A., HUANG, X., EBERT, D., MILLS, C., GUO, X. & THOMAS, P. D. 2019. Protocol Update for large-scale genome and gene function analysis with the PANTHER classification system (v.14.0). *Nat Protoc,* 14**,** 703-721.

MITSOGIANNIS, M. D., LITTLE, G. E. & MITCHELL, K. J. 2017. Semaphorin-Plexin signaling influences early ventral telencephalic development and thalamocortical axon guidance. *Neural Dev,* 12**,** 6.

MIYOSHI, G. & FISHELL, G. 2012. Dynamic FoxG1 expression coordinates the integration of multipolar pyramidal neuron precursors into the cortical plate. *Neuron,* 74**,** 1045-58.

MOEN, M. J., ADAMS, H. H., BRANDSMA, J. H., DEKKERS, D. H., AKINCI, U., KARKAMPOUNA, S., QUEVEDO, M., KOCKX, C. E., OZGUR, Z., VAN, I. W. F., DEMMERS, J. & POOT, R. A. 2017. An interaction network of mental disorder proteins in neural stem cells. *Transl Psychiatry,* 7**,** e1082.

MOLYNEAUX, B. J., ARLOTTA, P., MENEZES, J. R. & MACKLIS, J. D. 2007. Neuronal subtype specification in the cerebral cortex. *Nat Rev Neurosci,* 8**,** 427-37.

PAGE, S. C., HAMERSKY, G. R., GALLO, R. A., RANNALS, M. D., CALCATERRA, N. E., CAMPBELL, M. N., MAYFIELD, B., BRILEY, A., PHAN, B. N., JAFFE, A. E. & MAHER, B. J. 2017. The schizophrenia- and autism-associated gene, transcription factor 4 regulates the columnar distribution of layer 2/3 prefrontal pyramidal neurons in an activity-dependent manner. *Mol Psychiatry*, 23, 304–315.

PAUL, L. K., BROWN, W. S., ADOLPHS, R., TYSZKA, J. M., RICHARDS, L. J., MUKHERJEE, P. & SHERR, E. H. 2007. Agenesis of the corpus callosum: genetic, developmental and functional aspects of connectivity. *Nat Rev Neurosci,* 8**,** 287-99.

PILZ, D. T., MATSUMOTO, N., MINNERATH, S., MILLS, P., GLEESON, J. G., ALLEN, K. M., WALSH, C. A., BARKOVICH, A. J., DOBYNS, W. B., LEDBETTER, D. H. & ROSS, M. E. 1998. LIS1 and XLIS (DCX) mutations cause most classical lissencephaly, but different patterns of malformation. *Hum Mol Genet,* 7**,** 2029-37.

PRINGSHEIM, M., MITTER, D., SCHRODER, S., WARTHEMANN, R., PLUMACHER, K., KLUGER, G., BAETHMANN, M., BAST, T., BRAUN, S., BUTTEL, H. M., CONOVER, E., COURAGE, C., DATTA, A. N., EGER, A., GREBE, T. A., HASSE-WITTMER, A., HERUTH,

M., HOFT, K., KAINDL, A. M., KARCH, S., KAUTZKY, T., KORENKE, G. C., KRUSE, B., LUTZ, R. E., OMRAN, H., PATZER, S., PHILIPPI, H., RAMSEY, K., RATING, T., RIESS, A., SCHIMMEL, M., WESTMAN, R., ZECH, F. M., ZIRN, B., ULMKE, P. A., SOKPOR, G., TUOC, T., LEHA, A., STAUDT, M. & BROCKMANN, K. 2019. Structural brain anomalies in patients with FOXG1 syndrome and in Foxg1+/- mice. *Ann Clin Transl Neurol,* 6**,** 655-668.

RAO, N. P., VENKATASUBRAMANIAN, G., ARASAPPA, R. & GANGADHAR, B. N. 2011. Relationship between corpus callosum abnormalities and schneiderian first-rank symptoms in antipsychotic-naive schizophrenia patients. *J Neuropsychiatry Clin Neurosci,* 23**,** 155-62.

REIPRICH, S. & WEGNER, M. 2015. From CNS stem cells to neurons and glia: Sox for everyone. *Cell Tissue Res,* 359**,** 111-24.

RICHARDS, L. J., PLACHEZ, C. & REN, T. 2004. Mechanisms regulating the development of the corpus callosum and its agenesis in mouse and human. *Clin Genet,* 66**,** 276-89.

ROHM, B., OTTEMEYER, A., LOHRUM, M. & PUSCHEL, A. W. 2000. Plexin/neuropilin complexes mediate repulsion by the axonal guidance signal semaphorin 3A. *Mech Dev,* 93**,** 95-104.

SCHREIBER, J., ENDERICH, J., SOCK, E., SCHMIDT, C., RICHTER-LANDSBERG, C. & WEGNER, M. 1997. Redundancy of class III POU proteins in the oligodendrocyte lineage. *J Biol Chem,* 272**,** 32286-93.

SEPP, M., KANNIKE, K., EESMAA, A., URB, M. & TIMMUSK, T. 2011. Functional diversity of human basic helix-loop-helix transcription factor TCF4 isoforms generated by alternative 5' exon usage and splicing. *PLoS One,* 6**,** e22138.

SIFFREDI, V., ANDERSON, V., LEVENTER, R. J. & SPENCER-SMITH, M. M. 2013. Neuropsychological profile of agenesis of the corpus callosum: a systematic review. *Dev Neuropsychol,* 38**,** 36-57.

SNIJDERS BLOK, L., KLEEFSTRA, T., VENSELAAR, H., MAAS, S., KROES, H. Y., LACHMEIJER, A. M. A., VAN GASSEN, K. L. I., FIRTH, H. V., TOMKINS, S., BODEK, S., STUDY, D. D. D., OUNAP, K., WOJCIK, M. H., CUNNIFF, C., BERGSTROM, K., POWIS, Z., TANG, S., SHINDE, D. N., AU, C., IGLESIAS, A. D., IZUMI, K., LEONARD, J., ABOU TAYOUN, A., BAKER, S. W., TARTAGLIA, M., NICETA, M., DENTICI, M. L., OKAMOTO, N., MIYAKE, N., MATSUMOTO, N., VITOBELLO, A., FAIVRE, L., PHILIPPE, C., GILISSEN, C., WIEL, L., PFUNDT, R., DERIZIOTIS, P., BRUNNER, H. G. & FISHER, S. E. 2019. De Novo Variants Disturbing the Transactivation Capacity of POU3F3 Cause a Characteristic Neurodevelopmental Disorder. *Am J Hum Genet,* 105**,** 403-412.

SOCK, E., RETTIG, S. D., ENDERICH, J., BOSL, M. R., TAMM, E. R. & WEGNER, M. 2004. Gene targeting reveals a widespread role for the high-mobility-group transcription factor Sox11 in tissue remodeling. *Mol Cell Biol,* 24**,** 6635-44.

STEFANSSON, H., OPHOFF, R. A., STEINBERG, S., ANDREASSEN, O. A., CICHON, S., RUJESCU, D., WERGE, T., PIETILAINEN, O. P., MORS, O., MORTENSEN, P. B., SIGURDSSON, E., GUSTAFSSON, O., NYEGAARD, M., TUULIO-HENRIKSSON, A., INGASON, A., HANSEN, T., SUVISAARI, J., LONNQVIST, J., PAUNIO, T., BORGLUM, A. D., HARTMANN, A., FINK-JENSEN, A., NORDENTOFT, M., HOUGAARD, D., NORGAARD-PEDERSEN, B., BOTTCHER, Y., OLESEN, J., BREUER, R., MOLLER, H. J., GIEGLING, I., RASMUSSEN, H. B., TIMM, S., MATTHEISEN, M., BITTER, I., RETHELYI, J. M., MAGNUSDOTTIR, B. B., SIGMUNDSSON, T., OLASON, P., MASSON, G., GULCHER, J. R., HARALDSSON, M., FOSSDAL, R., THORGEIRSSON, T. E., THORSTEINSDOTTIR, U., RUGGERI, M., TOSATO, S., FRANKE, B., STRENGMAN, E., KIEMENEY, L. A., GENETIC, R., OUTCOME IN, P., MELLE, I., DJUROVIC, S., ABRAMOVA, L., KALEDA, V., SANJUAN, J., DE FRUTOS, R., BRAMON, E., VASSOS, E., FRASER, G., ETTINGER, U., PICCHIONI, M., WALKER, N., TOULOPOULOU, T., NEED, A. C., GE, D., YOON, J. L., SHIANNA, K. V., FREIMER, N. B., CANTOR, R. M., MURRAY, R., KONG, A., GOLIMBET, V., CARRACEDO, A., ARANGO, C., COSTAS, J., JONSSON, E. G., TERENIUS, L., AGARTZ, I.,

PETURSSON, H., NOTHEN, M. M., RIETSCHEL, M., MATTHEWS, P. M., MUGLIA, P., PELTONEN, L., ST CLAIR, D., GOLDSTEIN, D. B., STEFANSSON, K. & COLLIER, D. A. 2009. Common variants conferring risk of schizophrenia. *Nature,* 460**,** 744-7.

STEINBERG, S., DE JONG, S., IRISH SCHIZOPHRENIA GENOMICS, C., ANDREASSEN, O. A., WERGE, T., BORGLUM, A. D., MORS, O., MORTENSEN, P. B., GUSTAFSSON, O., COSTAS, J., PIETILAINEN, O. P., DEMONTIS, D., PAPIOL, S., HUTTENLOCHER, J., MATTHEISEN, M., BREUER, R., VASSOS, E., GIEGLING, I., FRASER, G., WALKER, N., TUULIO-HENRIKSSON, A., SUVISAARI, J., LONNQVIST, J., PAUNIO, T., AGARTZ, I., MELLE, I., DJUROVIC, S., STRENGMAN, E., GROUP, JURGENS, G., GLENTHOJ, B., TERENIUS, L., HOUGAARD, D. M., ORNTOFT, T., WIUF, C., DIDRIKSEN, M., HOLLEGAARD, M. V., NORDENTOFT, M., VAN WINKEL, R., KENIS, G., ABRAMOVA, L., KALEDA, V., ARROJO, M., SANJUAN, J., ARANGO, C., SPERLING, S., ROSSNER, M., RIBOLSI, M., MAGNI, V., SIRACUSANO, A., CHRISTIANSEN, C., KIEMENEY, L. A., VELDINK, J., VAN DEN BERG, L., INGASON, A., MUGLIA, P., MURRAY, R., NOTHEN, M. M., SIGURDSSON, E., PETURSSON, H., THORSTEINSDOTTIR, U., KONG, A., RUBINO, I. A., DE HERT, M., RETHELYI, J. M., BITTER, I., JONSSON, E. G., GOLIMBET, V., CARRACEDO, A., EHRENREICH, H., CRADDOCK, N., OWEN, M. J., O'DONOVAN, M. C., WELLCOME TRUST CASE CONTROL, C., RUGGERI, M., TOSATO, S., PELTONEN, L., OPHOFF, R. A., COLLIER, D. A., ST CLAIR, D., RIETSCHEL, M., CICHON, S., STEFANSSON, H., RUJESCU, D. & STEFANSSON, K. 2011. Common variants at VRK2 and TCF4 conferring risk of schizophrenia. *Hum Mol Genet,* 20**,** 4076-81.

STUART, T., BUTLER, A., HOFFMAN, P., HAFEMEISTER, C., PAPALEXI, E., MAUCK, W. M., 3RD, HAO, Y., STOECKIUS, M., SMIBERT, P. & SATIJA, R. 2019. Comprehensive Integration of Single-Cell Data. *Cell,* 177**,** 1888-1902 e21.

TZENG, M., DU SOUICH, C., CHEUNG, H. W. & BOERKOEL, C. F. 2014. Coffin-Siris syndrome: phenotypic evolution of a novel SMARCA4 mutation. *Am J Med Genet A,* 164A**,** 1808-14.

WILSON, B. J., HARADA, R., LEDUY, L., HOLLENBERG, M. D. & NEPVEU, A. 2009. CUX1 transcription factor is a downstream effector of the proteinase-activated receptor 2 (PAR2). *J Biol Chem,* 284**,** 36-45.

YAP, C. C., DIGILIO, L., MCMAHON, L., ROSZKOWSKA, M., BOTT, C. J., KRUCZEK, K. & WINCKLER, B. 2016. Different Doublecortin (DCX) Patient Alleles Show Distinct Phenotypes in Cultured Neurons: EVIDENCE FOR DIVERGENT LOSS-OF-FUNCTION AND "OFF-PATHWAY" CELLULAR MECHANISMS. *J Biol Chem,* 291**,** 26613-26626.

YU, G., WANG, L. G., YAN, G. R. & HE, Q. Y. 2015. DOSE: an R/Bioconductor package for disease ontology semantic and enrichment analysis. *Bioinformatics,* 31**,** 608-9.

ZWEIER, C., PEIPPO, M. M., HOYER, J., SOUSA, S., BOTTANI, A., CLAYTON-SMITH, J., REARDON, W., SARAIVA, J., CABRAL, A., GOHRING, I., DEVRIENDT, K., DE RAVEL, T., BIJLSMA, E. K., HENNEKAM, R. C., ORRICO, A., COHEN, M., DREWEKE, A., REIS, A., NURNBERG, P. & RAUCH, A. 2007. Haploinsufficiency of TCF4 causes syndromal mental retardation with intermittent hyperventilation (Pitt-Hopkins syndrome). *Am J Hum Genet,* 80**,** 994-1001.

Figures

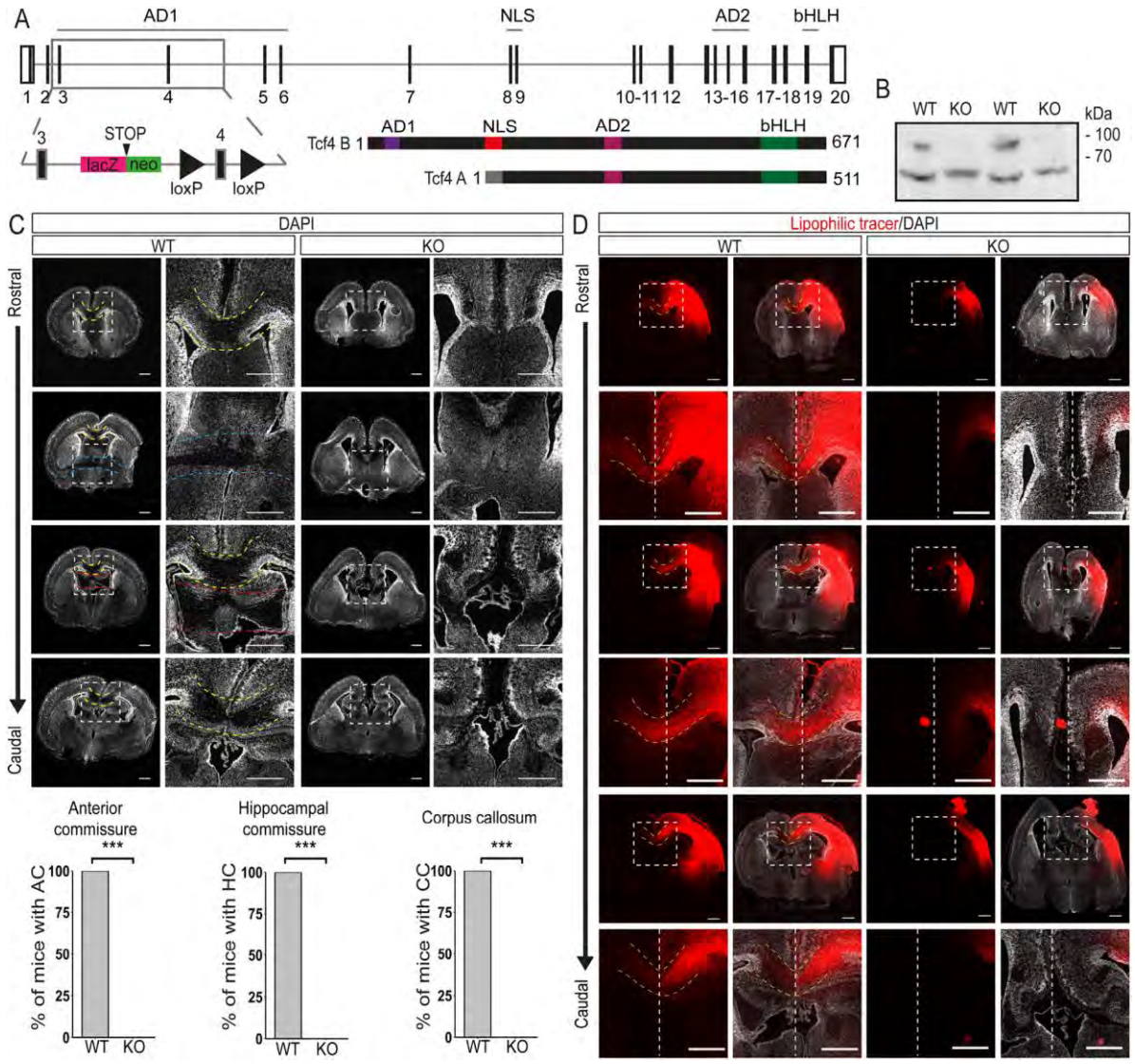

Figure 1. Loss of *Tcf4* disrupts commissure formation

A Schematic representation of the *Tcf4* gene, the `knockout-first´ conditional allele and the two main TCF4 isoforms.

B Western Blot analysis of neocortical extracts from E18.5 WT or *Tcf4KO* mice using anti-TCF4 antibody. The blot presented is cropped. The longest isoform of TCF4 is missing in the KO samples (n = 3).

C Representative overview and magnification images (DAPI) of brain sections at P0 showing the loss of the three commissure systems in *Tcf4KO* mice. Images on the right are magnification of the area marked with a white rectangle. Yellow dotted lines indicate the CC crossing the midline. Blue dotted lines indicate the AC and red dotted lines the HC. Quantification of animals showing a commissural system is presented below (n = 8, mean ± s.d).

D Representative overview and magnification images of lipophilic tracer (red) treated brains at P0 without or with DAPI staining (white). Images below the overview images are magnification of the area marked with a white rectangle. White dotted lines indicate the midline and yellow dotted lines the CC. Note that only in WT animals, lipophilic tracer signal can be detected in the contralateral hemispheres (n = 3).

All scale bars, 500 µm. For more overview and magnification images see Figs S1 and S2.

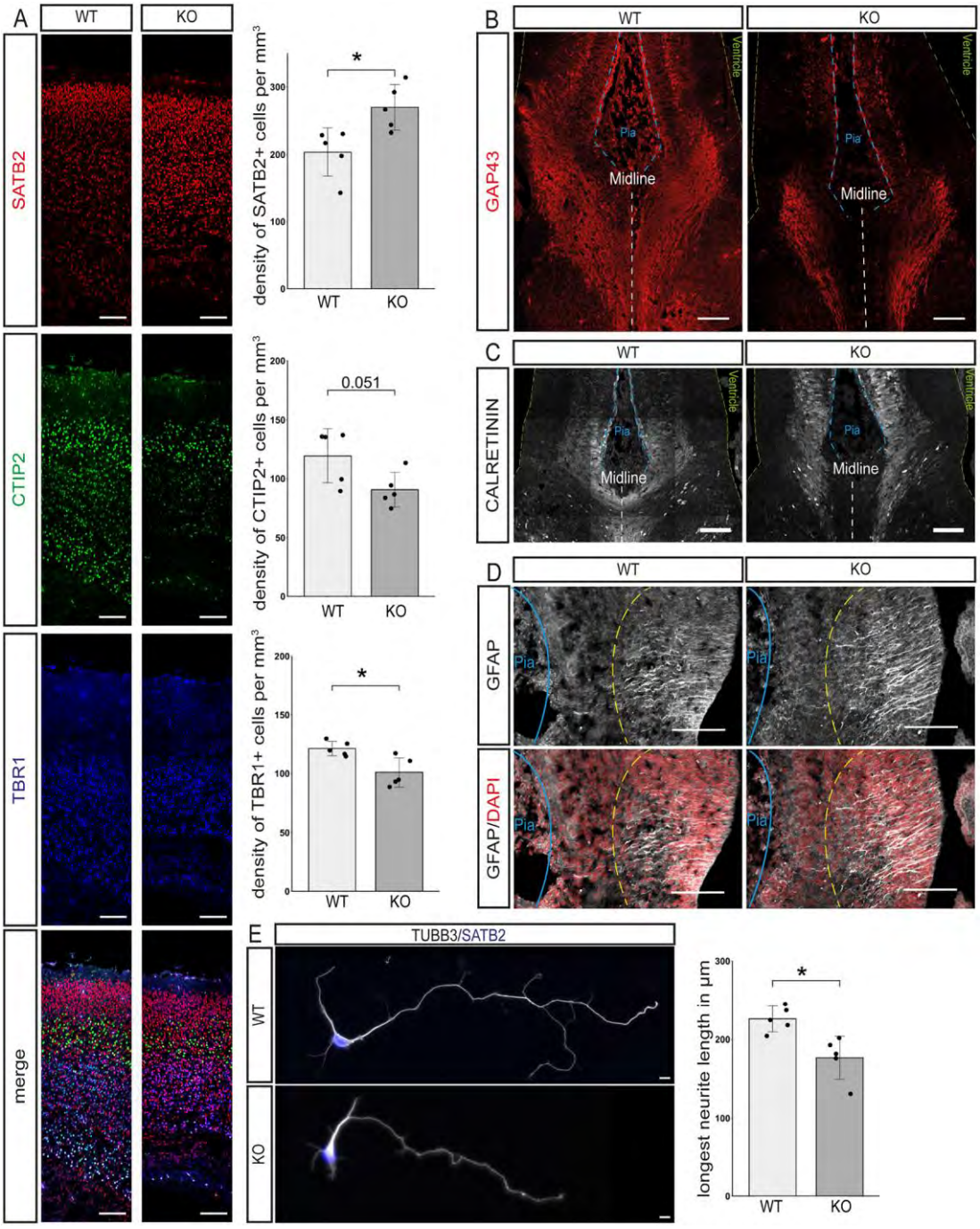

Figure 2. Loss of Tcf4 disrupts cortical layering and neurite outgrowth

A Representative images of the neuronal markers SATB2 (upper layers, red), CTIP2 (layer V, green) and TBR1 (layer VI, blue) and the quantification of the density of cells expressing these markers in mm^3. A significant increase in SATB2+ neurons is observable as is a significant decrease in TBR1+ cells (n = 5, mean ±s.d; p-values were determined with two-tailed student´s t-tests; SATB2+ cells in mm^3: WT 203 ± 32; KO 270 ± 30; p = 0.017; CTIP2+

in mm^3: WT 119 ± 21; KO 91 ± 13; p = 0.051; TBR1+ cells in mm^3: WT 121 ± 5; KO 101 ± 11; p = 0.018). Scale bar, 100µm

B Representative images for GAP43 at the midline of E16.5 mouse brains. Green dotted lines represent the ventricular surface, blue dotted lines the pial surface and white dotted lines the midline. (n = 3). Scale bar, 100µm

C Representative images of CALRETININ expression at the midline at E16.5. Green dotted lines represent the ventricular surface, blue dotted lines the pial surface and white dotted lines represent the midline. (n = 3). Scale bar, 100µm

D Representative images of GFAP stainings at E16.5. Blue lines represent the pial surface. Yellow dotted lines represent the end of the processes of the glial wedge glia (n = 3). Scale bar, 100µm

E Representative images of primary cortical neurons stained with TUBB3 (grey) and SATB2 (blue) and the quantification of the length of the longest neurite. *Tcf4*KO neurons show a reduced neurite length (n=5; 20 neurons per animal; Longest neurite length in µm: WT 226,02 ± 14,76; KO 176,59 ± 24,45; p-value = 0.012). Scale bare, 10µm

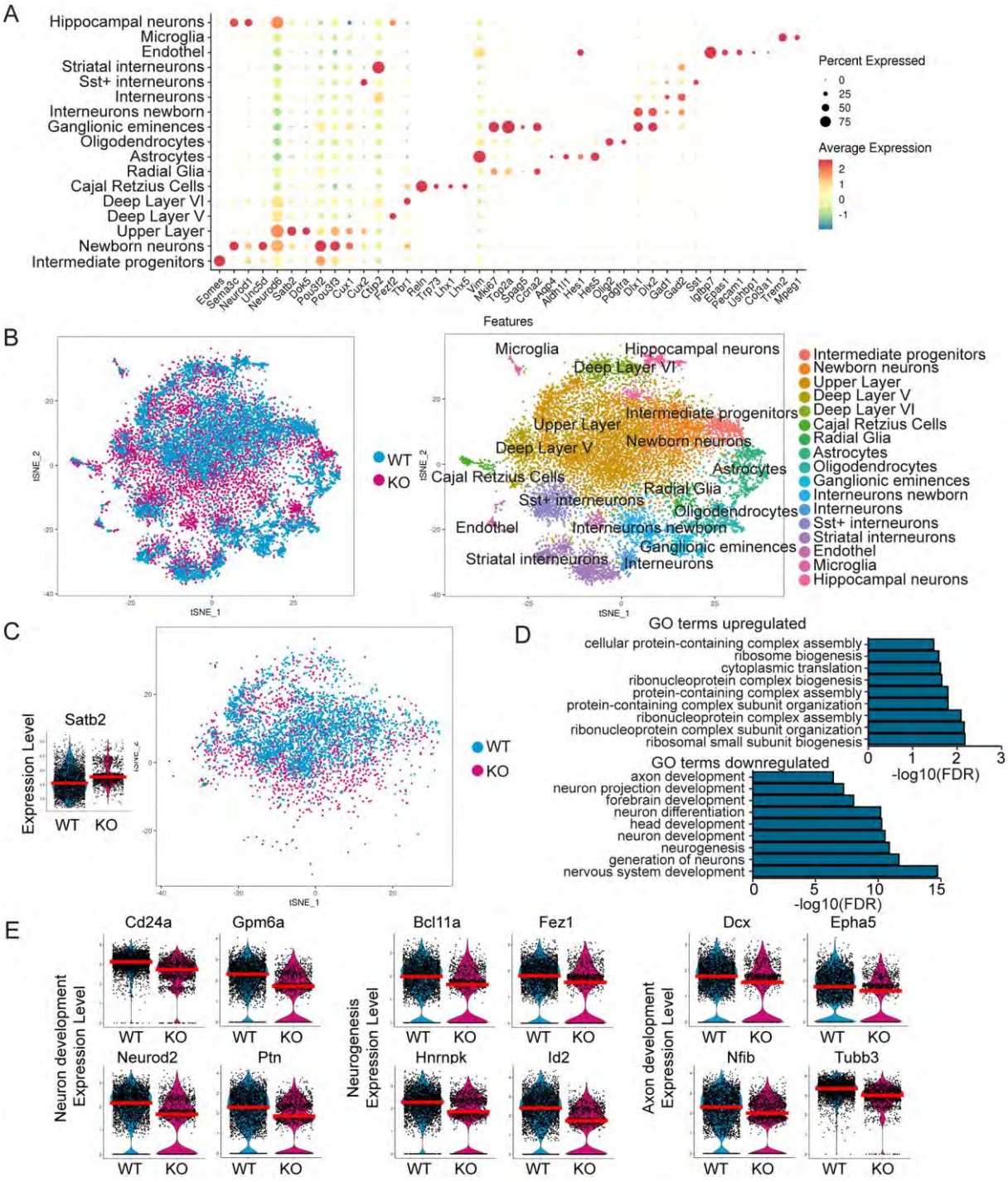

Figure 3. Single-cell RNA Sequencing of E18.5 neocortices from WT and *Tcf4KO* mice

A Dot-Plot of cell clusters (y-axis) and a selection of marker used to assign the cell type (x-axis).

B tSNE-Plot coloured by genotype (left) and cluster identity (right).

C tSNE-Plot of *Satb2* expressing glutamatergic cells used for further analysis. Violin Plot of *Satb2* expression in the *Satb2* cluster. The red line depicts the median.

D Selection out of the first 50 GO terms associated with up- and downregulated genes in *Satb2* expressing glutamatergic cells. GO terms for neurogenesis, neuronal differentiation and axon development were downregulated in the *Tcf4*KO cells.

E Violin Plot of differentially expressed genes in the *Satb2* cluster that are associated to neurogenesis and neuron and axon development. The red line depicts the median.

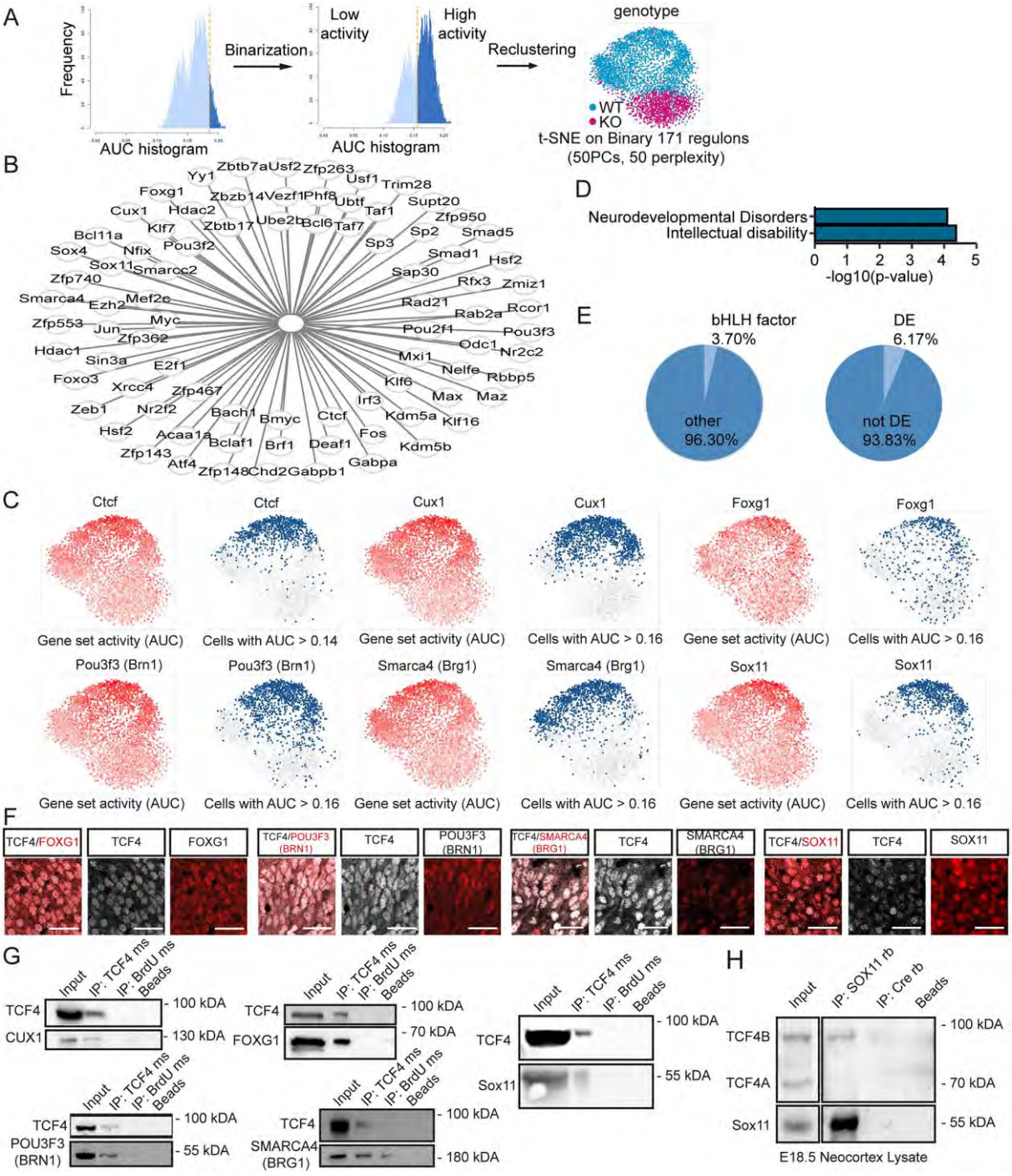

Figure 4. Gene regulatory network analysis of SATB2 expressing cells

A Scheme of the workflow used to recluster cells after GRN analysis and resulting tSNE-Plot of the *Satb2* cluster. Regulons are binarized and reclustered accordingly. WT and KO cells segregated based on GRN activity with only minor overlap.

B Differentially active regulons of the *Satb2* cluster that may be possible interactors of TCF4.

C tSNE-Plots showing the regulon activity of *Ctcf, Cux1, Foxg1, Pou3f3* (also known as *Brn1*), *Smarca4* (also known as *Brg1*) and *Sox11* in a continuous scale (left, red) or binarized (right, blue). The regulons are highly active in the WT cells with only a small number of KO cells showing a high expression.

D Selection of diseases association enriched in the list of differentially active regulons.

E Pie charts depicting the percentage of bHLH factors and differentially expressed regulators in the differentially active regulons.

F Representative images of TCF4 (white) and FOXG1, POU3F3 (BRN1), SMARCA4 (BRG1) and SOX11 (all in red) in the upper third of E18.5 WT cortices. Note the expression in the same nuclei. Scale bar, 50 µm

G Co-immunoprecipitation assay using anti-TCF4 antibody conducted with HEK cell extract after overexpression of TCF4 and CUX1, FOXG1, POU3F3 (BRN1), SMARCA4 (BRG1) and SOX11 in HEK cells. Upper panels: detection with anti-TCF4 antibody. Lower panels: detection with anti-Cux1, anti-FOXG1, anti-BRN1, anti-BRG1 or anti-SOX11 antibody. The blots presented are cropped. All proteins were co-immunoprecipitated with TCF4, but not with an isotype control for IgG or Agarose A Beads alone except for BRN-1 which was precipitated to a small amount by the isotope control IgG. The interactions were confirmed in three independent biological replicates, (n = 3); ms = antibody raised in mouse.

H Co-immunoprecipitation assay conducted with E18.5 cortex lysates using anti-SOX11 antibody. Upper panel: detection with anti-TCF4 antibody. Lower panel: detection with anti-SOX11 antibody. The blots presented are cropped. TCF4B was co-immunoprecipitated with SOX11, but not with an isotype control for IgG and Agarose A Beads alone. The interaction was confirmed in three independent biological replicates (n = 3); rb = antibody raised in rabbit.

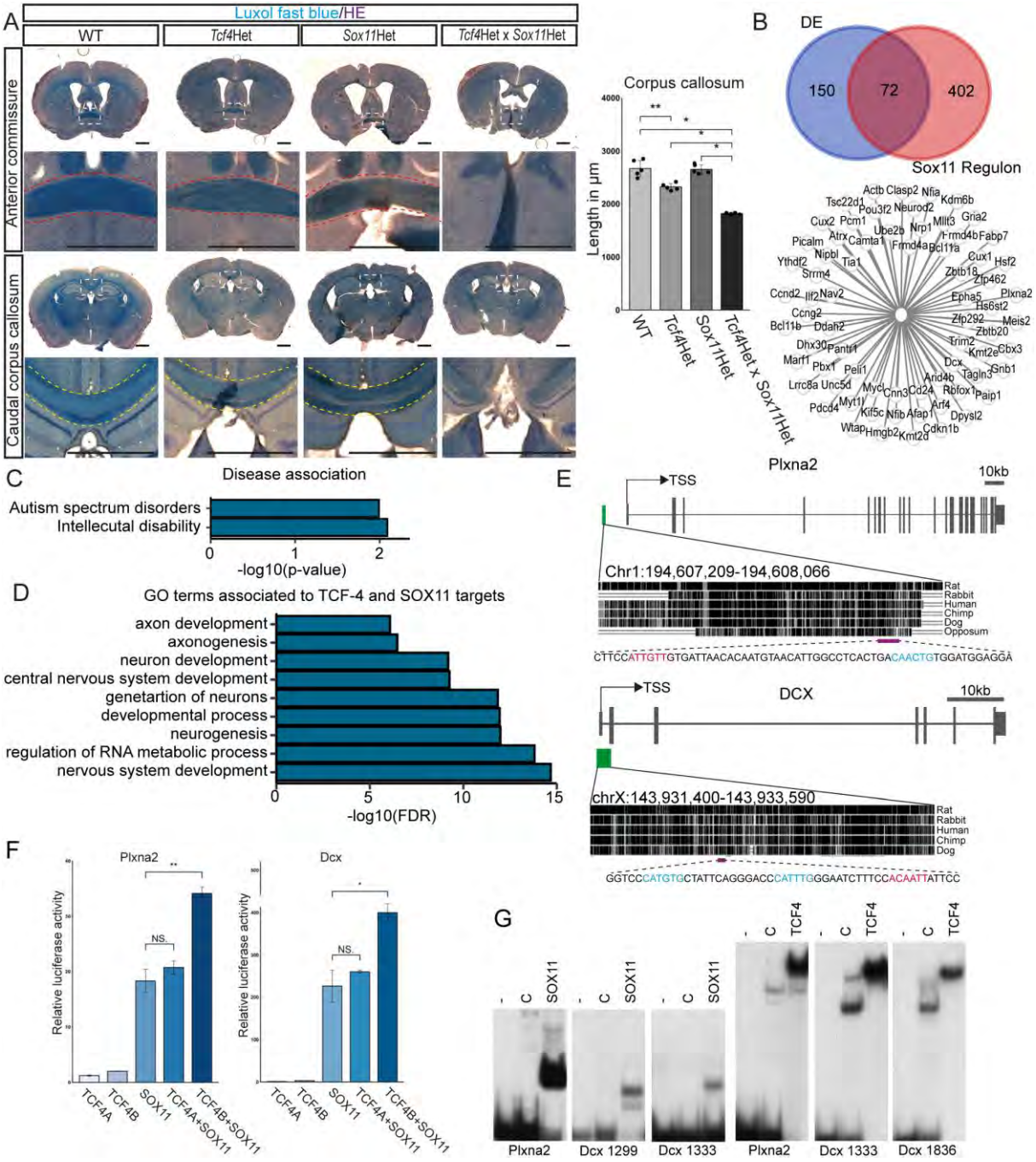

Figure 5. TCF4 and SOX11 act synergistically in corpus callosum formation

A Representative overview images of Luxol fast blue stainings at the position of the AC and the caudal body of the CC. Images below the overview images are magnification of the area marked with a white rectangle. Yellow dotted lines indicate the CC crossing the midline. Red dotted lines indicate the AC. In *Tcf4* and *Sox11* double haploinsufficient mice agenesis of the AC and agenesis of the splenium and caudal part of the body of the CC can be observed. Quantification of slices showing a corpus callosum is presented at the right. Scale bar, 1000 µm, (n=5, p-values were determined with Mann-Whitney-U tests ; mean ±s.d, WT 2664µm ±

137.64; *Tcf4*Het 2320 ± 56.57; Sox11Het 2648 ± 77.56; Tcf4Het x Sox11Het 1816 ± 19.60; WT vs *Tcf4*Het: p-value = 0.008; WT vs *Tcf4*Het x *Sox11*Het: p-value = 0.011; *Tcf4*Het vs *Tcf4*Het x *Sox11*Het: p-value = 0.011; *Sox11*Het vs *Tcf4*Het x *Sox11*Het: p-value = 0.011). For more overview and magnification images see Fig. S7.

B Venn diagram of the overlap of differentially expressed genes and the targets of the Sox11 regulon in the *Satb2* cluster. Possible common targets are depicted on the right.

C Selection of diseases association enriched in the list of common targets of TCF4 and SOX11 in the *Satb2* cluster.

D Selection of GO terms associated with the common targets of TCF4 and SOX11 in the *Satb2* cluster. GO terms for neurogenesis, neuronal differentiation and axonogenesis were enriched.

E Schematic representation of *Plxna2* and *Dcx* gene and the location of the ECRs with TCF4 and SOX11 binding capacity (green box) relative to the transcriptional start site (TSS). The magenta box indicates the regions with possible binding sites of TCF4 (blue) and SOX11 (red). For DNA-Sequences see Fig. S9.

F Relative luciferase reporter gene activity under the control of the regulatory regions from the *Plxna2* and *Dcx* in transiently transfected HEK cells co-expressing TCF4A, TCF4B, SOX11 and a combination of either TCF4A or TCF4B with SOX11 (n = 3, p-values were determined with two-tailed student´s t-tests; presented as mean ± s.d., transfection with empty CAG-GFP vector was set to 1 for each regulatory region; *Dcx*: SOX11 vs. TCF4A+SOX11: p-value = 0.387; SOX11 vs. TCF4B+SOX11: p-value = 0.006; *Plxna2*: SOX11 vs. TCF4A+SOX11: p-value = 0.462; SOX11 vs. TCF4B+SOX11: p-value = 0.025).

G For electrophoretic mobility shift assay (EMSA), oligonucleotides containing potential Sox11 binding sites and E-Boxes from the *Plxna2* and *Dcx* ECRs (for sequences, see Fig. 5E or Fig. S9) were incubated without cell extract (−), or in the presence of extracts from HEK293 cells transfected with empty expression vector (C) or expression vector for the Sox11 high-mobility-group domain (amino acids 38–126 of Sox11) or the bHLH domain of TCF4B (amino acids 491-617 of TCF4B).

Supplemental Materials and Methods

Proximity ligation assay

WT neurospheres derived from the subventricular zone of E14.5 neocortices were used for all experiments. To generate neurosphere cultures, time-pregnant mice were killed by cervical dislocation at E14.5 and neocortices of single embryos were dissected under a binocular and immediately transferred to ice cold PBS. After removal of PBS the tissue was incubated in 5 ml dissociation medium (1x HBSS, 5.4mg/ml Glucose, 15mM HEPES, Trypsin, Hyaloronidase) for 15 min at 37°C. The solution was then gently triturated ten times with a glass pipette and incubated for another 15 min at 37°C. 5 ml of ice cold solution 3 (4%BSA, 20mM HEPES in EBSS) was added, followed by a passage through a 70 µm strainer and centrifugation at 300 g for 5 min. The supernatant was discarded and cells were resuspended in 10 ml of ice cold solution 2 (0.5xHBSS, 90mM Sucrose). The solution was centrifuged again for 10 min at 400 g, the supernatant was removed and cells were mixed with 2 ml of ice cold solution 3. The cell suspension was then gently layered on top of 12 ml ice cold solution 3 and centrifuged at 300g for 10 min. Neurosphere cultures were obtained by disposition of the supernatant and resuspension in neurosphere media [DMEM F12 Glutamax (GIBCO) medium with 1xNeurobrew-21 (MACS Miltenyi Biotec), 1x penicillin/Streptomycin (GIBCO), 8 mM HEPES and 10 ng/ml EGF and 10 ng/ml FGF (Peprotech)] and cultivation at 37°C, 5% CO_2. Cells were split after a dark spot became apparent in the middle of the spheres. Neurospheres were transferred into a 15 ml falcon and centrifuged at 500 rpm. The supernatant was discarded, the cells were resuspended in 1 ml Accutase (Millipore) and then incubated at 37°C for 5 min. To dissociate the neurospheres into single cells, cells were triturated several times with a Pasteur glass pipette and incubated again for 5 min. Cells were centrifuged for 5 min at 1500 rpm and the Accutase was removed. Cells were washed two times in 5 ml PBS and centrifuged for 5 min at 1500 rpm. The cell pellet was resuspended in 1 ml neurosphere media and counted using a counting chamber. Cells were either passaged for expansion in flasks or 100 000 cells were seeded in PDL/laminin coated cover slips in 24 wells plates. The medium of seeded neurospheres was removed a day after seeding and medium without growth factors was added to the cells to trigger to trigger differentiation. On every third day the medium was changed. Cells were fixed at day 6 of differentiation. Proximity ligation assay was performed according to the manufactures instruction (Sigma Aldrich Chemie GmbH Munich, Germany) using [rb

BRN1 (kind gift of Elisabeth Sock) 1:500); rb BRG1 (Santa Cruz, sc10768) 1:100; ab rb FOXG1 (Abcam, ab18259) 1:500; ms TCF4 (Santa Cruz, sc393407) 1:100].

DAPI staining at P7

Free floating sections were washed two times with 1x PBS and incubated with DAPI for 10min followed by another two times washing 1x PBS. Slides were mounted with 60 µl Mowiol and stored at 4°C. To quantify the length of the corpus callosum, the slices were counted from the first slices to last slices showing a corpus callosum. Brains were serially cut into 30 µm sections.

In utero electroporation

Plasmid (pCAG-TCF4A-IRES-EGFP or tdTomato as control) was dissolved in saline to a concentration of 2 µg/µl with 0.05% Fast Green to monitor the injection. Pregnant ICR mice were anesthetized, and the uterine horns were exposed. Approximately 1 µl of DNA solution was injected into the lateral ventricle of embryos using a pulled glass micropipette. Each embryo within its uterus was placed between tweezer-type electrodes (CUY650P5), and 50 ms electronic pulses of 40 V were charged five times at 950 ms intervals using a square-pulse electroporator (CUY21SC; Nepa Gene Company). The uterine horns were placed back in the abdominal cavity, and the abdominal wall and skin were sewed with surgical sutures. Pups were harvested at P0.5 for immunohistochemistry. For each animal matching slides were divided into 10 bins and the number of CTIP2+ cells and marker positive cells was determined for each bin.

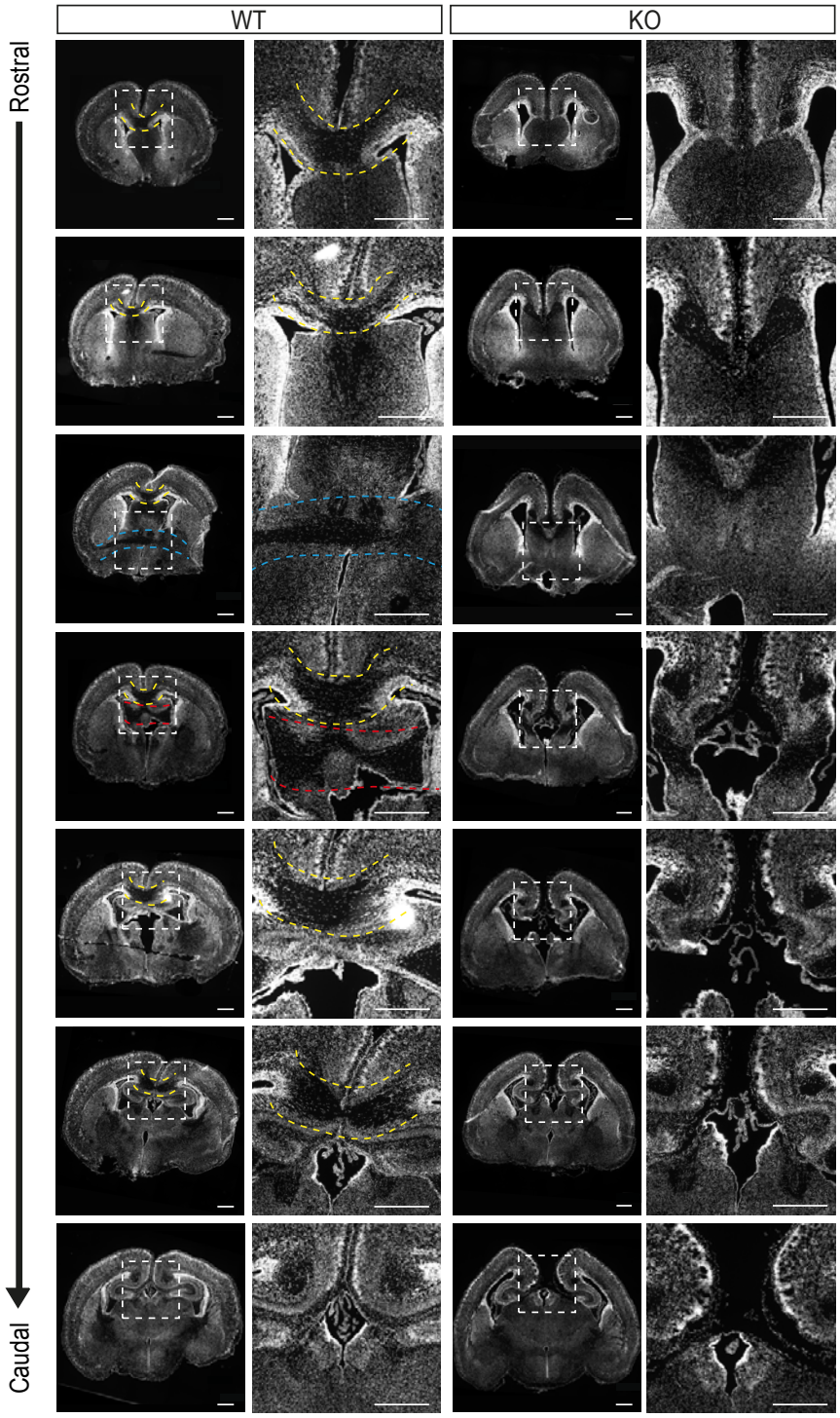

Figure S1. Overview images of the three forebrain commissures

Representative overview and magnification images of brain sections at P0 stained with DAPI showing the loss of the three commissure systems in *Tcf4KO* mice. Images on the right are magnification of the area marked with a with rectangle. Yellow dotted lines indicate the corpus callosum crossing the midline. Blue dotted lines indicate the anterior commissure and red dotted lines the hippocampal commissure. Scale bar, 500 µm.

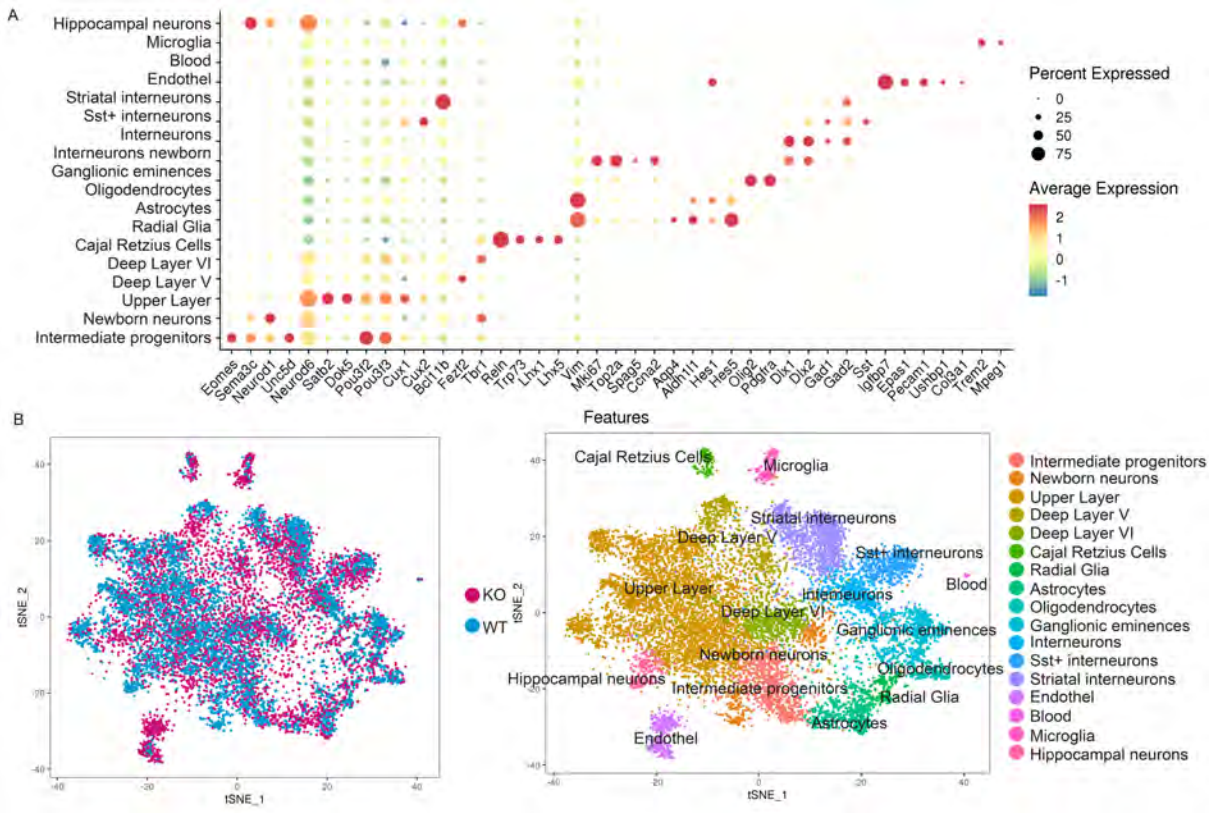

Figure S2. Clustering of the single cell dataset using the multiCCA approach

A Dot-Plot of cell clusters (y-axis) and representative marker used to assign the cell type (x-axis).

B tSNE-Plot coloured by genotype (left) and cluster identity (right).

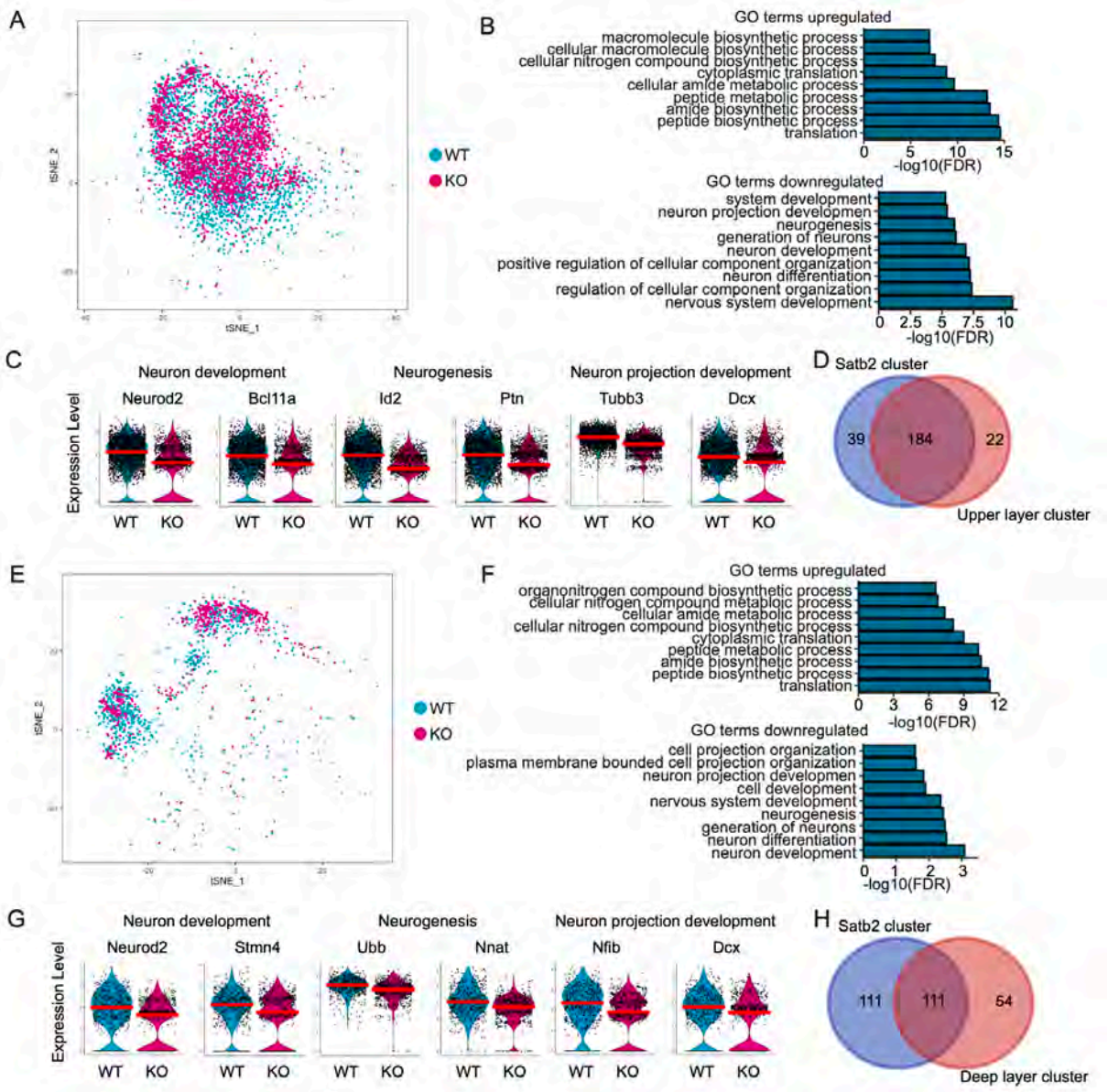

Figure S3. Differentially expressed gene analysis of the upper and deep layer cluster

A tSNE-Plot of the upper layer cluster used for further analysis.
B Selection out of the first 50 GO terms associated with up- and downregulated genes in the upper layer cluster. GO terms for neuron development, neurogenesis and neuron projection development were downregulated in the *Tcf4*KO cells.
C Violin Plots of differentially expressed genes in the upper layer cluster that are associated to neuron development, neurogenesis and neuron projection development. The red line depicts the median.
D Venn-Diagramm of the overlap of differentially expressed genes between the *Satb2* and UL cluster
E tSNE-Plot of deep layer cluster used for further analysis.
F Selection out of the first 50 GO terms associated with up- and downregulated genes in the deep layer cluster. GO terms for neuron development, neurogenesis and neuron projection development were downregulated in the *Tcf4*KO cells.
G Violin Plots of differentially expressed genes in the deep layer cluster that are associated to neuron development, neurogenesis and neuron projection development. The red line depicts the median.
H Venn-Diagramm of the overlap of differentially expressed genes between the *Satb2* and UL cluster

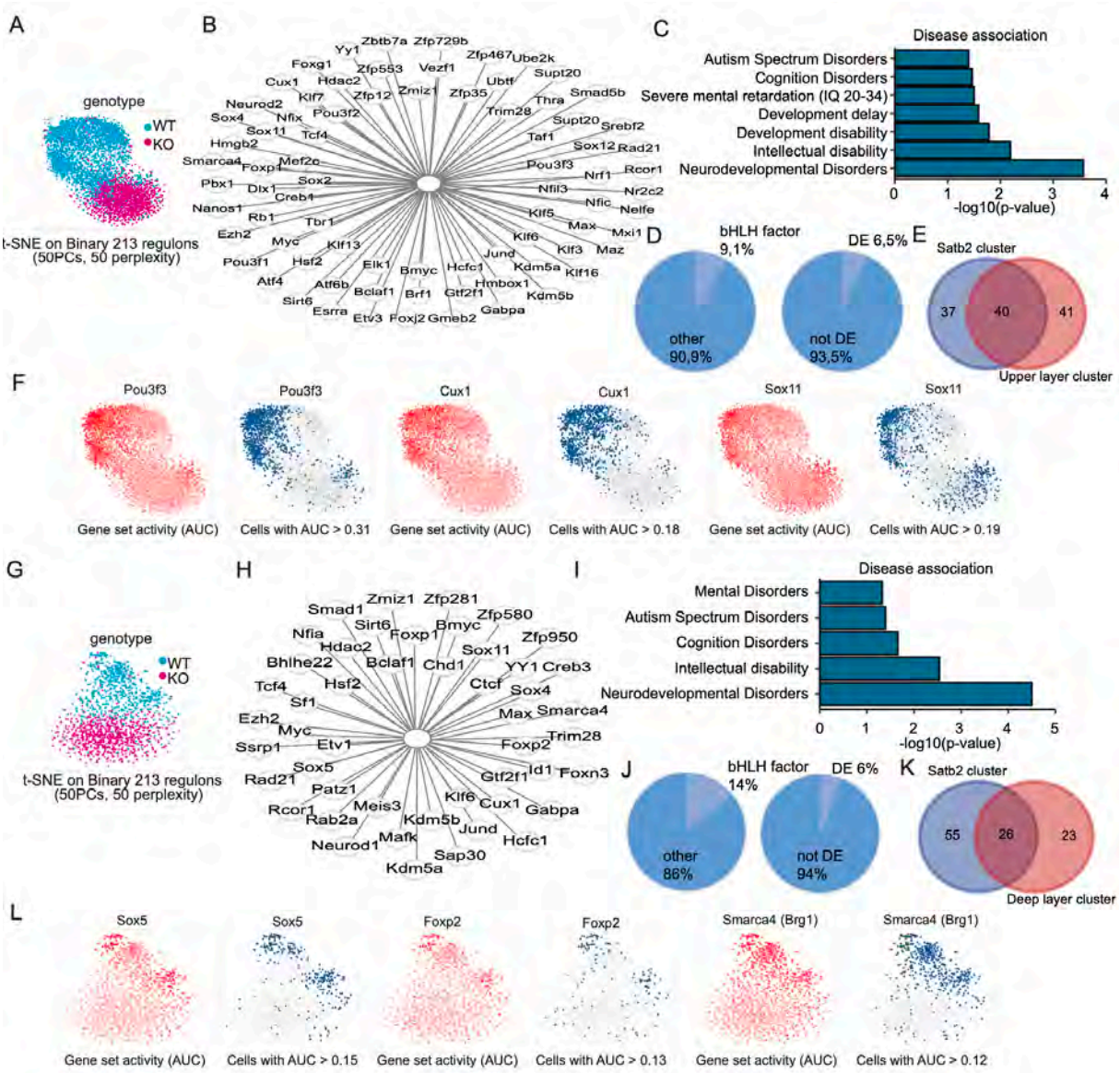

Figure S4. Gene regulatory network analyses of the upper and deep layer cluster

A tSNE-Plot of the upper layer cluster after GRN analysis. WT and KO cells segregated based on GRN activity with only minor overlap.
B Differentially active regulons of the upper layer cluster that may be possible interactors of TCF4.
C Selection of diseases association enriched in the list of differentially active regulons.
D Pie charts depicting the percentage of bHLH factors and differentially expressed regulators in the differentially active regulons.
E Venn-Diagramm of the overlap of differentially active regulons between the *Satb2* and UL cluster
F tSNE-Plots showing the regulon activity of *Pou3f3, Cux1* and *Sox11* in a continuous scale (left, red) or binarized (right, blue). The regulons are highly active in the WT cells with only a small number of KO cells showing a high expression.
G tSNE-Plot of the deep layer cluster after GRN analysis. WT and KO cells segregated based on GRN activity with only minor overlap.
H Differentially active regulons of the deep layer cluster that may be possible interactors of TCF4.
I Selection of diseases association enriched in the list of differentially active regulons.
J Pie charts depicting the percentage of bHLH factors and differentially expressed regulators in the differentially active regulons.
K Venn-Diagramm of the overlap of differentially active regulons between the *Satb2* and DL cluster
L tSNE-Plots showing the regulon activity of *Sox5, Foxp1* and *Smarca4* (also known as *Brg1*) in a continuous scale (left, red) or binarized (right, blue). The regulons are highly active in the WT cells with only a small number of KO cells showing a high expression.

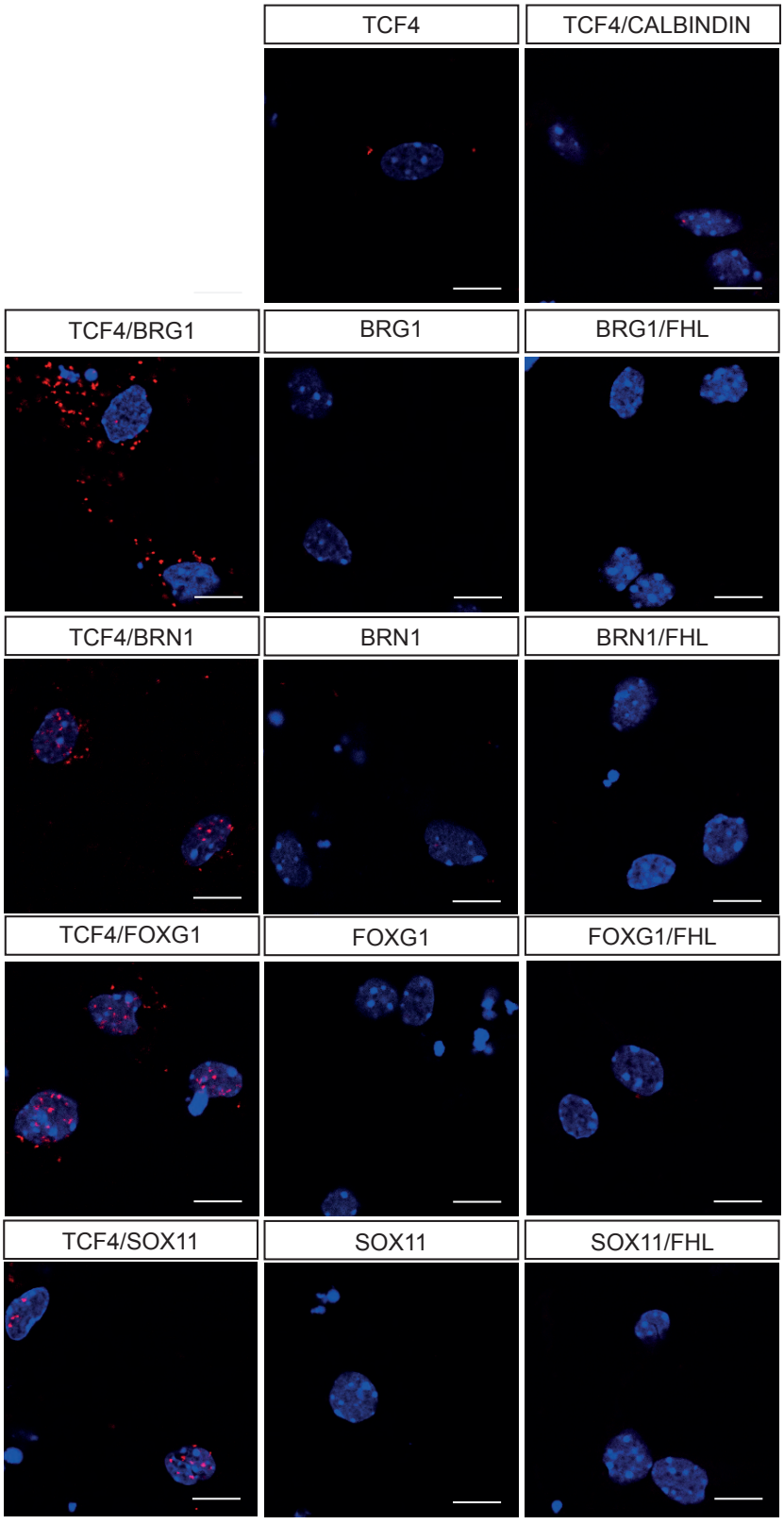

Figure S5. Proximity ligation assay in 6 days differentiated cortical neurospheres.

Left column: Proximity ligation assay using both mouse TCF4 and rabbit BRG1, BRN1, FOXG1 or SOX11 antibody. Middle column: Proximity ligation assay using only one antibody (ms TCF4, rb BRG1, rb BRN1, rb FOXG1 or rb SOX11) to control for unspecific amplification. Right column: Proximity ligation assay using mouse TCF4 and rabbit Calbindin or mouse FHL and rb BRG1, rb BRN1, rb FOXG1 or rb SOX11 to control for unspecific amplification. (n=3). ms = mouse; rb = rabbit.

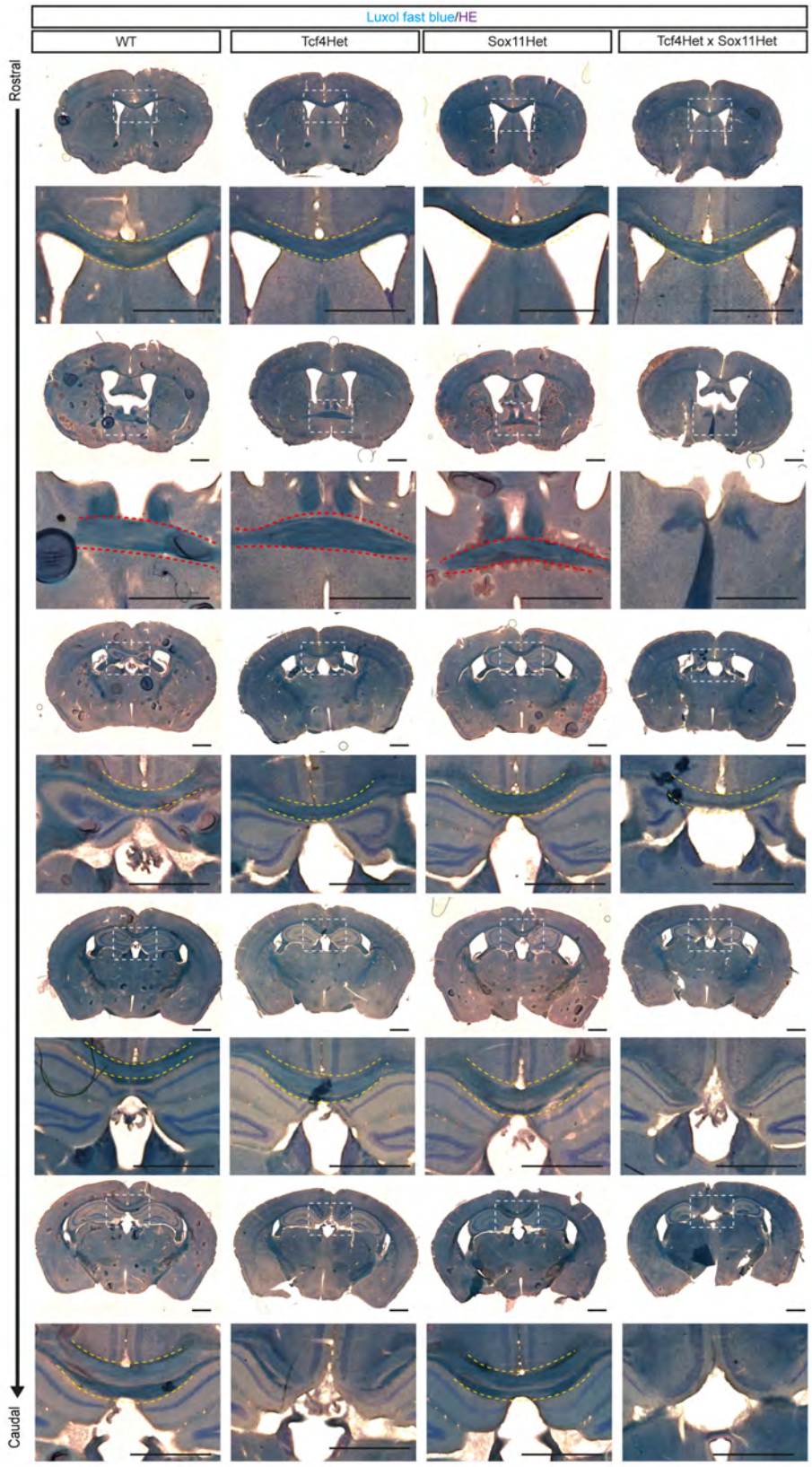

Figure S6. Overview images of Luxol fast blue stainings at P56

Representative overview and magnification images of Luxol fast blue stainings. Images below are magnification of the area marked with a white rectangle. Yellow dotted lines indicate the CC crossing the midline. Red dotted lines indicate the AC. In *Tcf4* and *Sox11* double haploinsufficient mice agenesis of the AC and agenesis of the splenium and caudal part of the body of the CC can be observed. Scale bar, 1000 µm, (n=5).

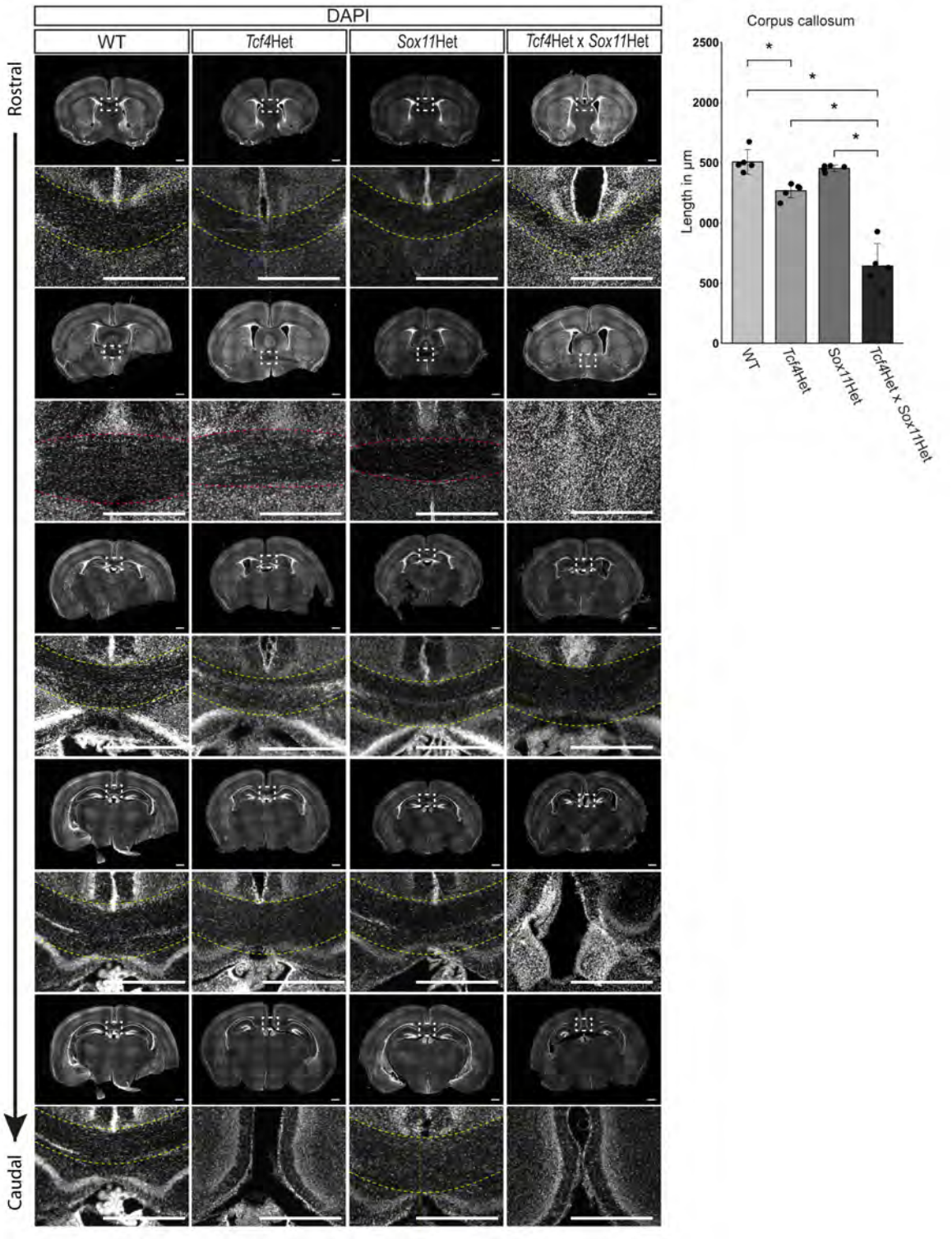

Figure S7. Overview images of DAPI stainings at P7

Representative overview and magnification images (DAPI) of brain sections at P7 showing the commissural system. Images below are magnification of the area marked with a white rectangle. Yellow dotted lines indicate the CC crossing the midline. Red dotted lines indicate the AC. In *Tcf4* and *Sox11* double haploinsufficient mice agenesis of the AC and agenesis of the splenium and caudal part of the body of the CC can be observed. Quantification of slices showing a corpus callosum is presented at the right. Scale bar, 1000 µm, (n=5, mean ± s.d, p-values were determined with Mann-Whitney-U test; WT 1506µm ± 91,78; *Tcf4*Het 1266 ± 51.61; Sox11Het 1452 ± 24; Tcf4Het x Sox11Het 642 ± 166,06; WT vs *Tcf4*Het: p-value = 0.012; WT vs *Tcf4*Het x *Sox11*Het: p-value 0.012; *Tcf4*Het vs *Tcf4*Het x *Sox11*Het: p-value = 0.012; *Sox11*Het vs *Tcf4*Het x *Sox11*Het: p-value = 0.011).

A Plxna2-ECR-Sequence:

CAGATTCTAAAGGTAAATCCCCAGAGAGGCATGCTTGAGGAAGTACTGAGGTGATTGCAGCACTGGACAG
CTGTGGGTTGGGCATGACACCTTCCAGACTCCAAGAGTAACCTGAGCAGAAGTTGAGGAGACAGGGGAT
CTTAGCTTTTTCCAGAGACAGAGGGTTGAAGGAGGAGGAGCTATGAGAAATGCAACAGGTACCAAGGGTA
GACCAAAATTATGAAAAGCATGAAAAGATGGCCTTTATCCCTCTAATGTTATGGCTATGTGGTGTTATTTTT
ATTCAAGGGAAGAAAAAAAAAAAAAGAAAGAAAGAAAAGAATGCATGCTGCTCACCCAAACATCAGGACAT
TCTGTCCCTCTGTGATTGTGCTTCATGAAAATGCTTTCCAGCAAAAAATGAGAAAGAATGATTAAGGGGAA
AAAAATAACTAGAGCCACATTCATTTCAGCTTCTCTGAAAGCACAGCAGGAGGAAGTGGCTATGTTTGCCA
AACTCCAGAAAAAGACACAATTGACAGGAGGCGGGGAGGGGAGGGTGAGGCAGCAGAGGGCATATGGA
GGAGGGGTACCCCTTGTTTTATTCTCCCCTGAAGATACAGTAAATAATGAAGAGGTGTGGTGCACGGAGG
AGAAATTACTTAACAGGGCCCTTTCAGGGAGGAAAGTGGAACTAAACCCAGTCTCCATCATTTGTTCTGAC
ATCCAACTCCCTGTTTACATGGGCGATCCCTGGAGCTGACACTCCACTCTGCTGTCACAAGTAGTCCTTGA
CTGGAGCCGATCATCTCAAAATAATGCCCTGAAGTTCTTCCATTGTTGTGATTAACACAATGTAACATTGGC
CTCACTGACAACTGTGGATGGAGGAAGATAGCCTGCAGACCTCCCTGATTGTTGGAGCCAGAAAAAGTCC
CAATTAGTCCACTGGGTGGCACTCTCACTAGGGTTCTCTGCATCTTTTCTGGCCCATGGTGTCCACCAAAG
AATTGATTCAG

B DCX-Promotor-Sequence:

TGACTTCGTTTAAAAAACAACCAGTGTTGGATGCATGAGCCGAAATGTTAAAAAATTTACATATTTTTTATTT
TCTTTGAAGAAGATAAAAAGAGGAGATCTGTAATTTCTAAGAAACTTGATTTGGCCTGCTGAGTCCAGCCA
CTAGGCAGAAGGTTTTAGCCAAGTAAAATTGCCAATTTTCTAAGAGAAAGGGCTAGCACATTGCTCATTAG
AGCATTCTGAGCTTGCCTGTGCAATCTTTTTTTTCCTACCCTGCAATTTCCTGTGCGTTATAAACGAAACCT
TTCTAGCTGTTAATGCAGGCTGTGAATTGAAGAAAAAAAAAGCATGTAATTAATCATAGGAGGTTGGGGGTG
TTCGCTAAGCTTCAGTTACAGGGGAGAAGCTGGACAAGGCACTAGGACCTAGAAGGCAACTATCCACCCT
GGCAGGAATTTCTTGCTTGGAGCTCAGACAACAAAGGCATAGAGAGATTGGTTTTCTTTCTCTCAGCATCT
CCACCCAACCAGCAGAAAACCGGTGAGTGGGGCTTTCGAGTGATTTTCAAGCAGAATGTAACAGATGTCA
ACCGGGAAAGCACAAGGCACACGGCTTTCTTTCTCTGTGTGTTCGCCTCTTTCTTCTCTTTTATTTGCCTTA
TTCTATAGGATTTTTGTCCTCTAAGATTCTACCTGGGATTTTCCTTTGGAAAAGTGAGTTTGTTGTTCCTTTG
TTTTCACTATGATGCTAATTTAGAATAATAGCACTTCTGATTCTAAAGCATAGCTTTATTTGCACAGCCTGCC
TGGGGAAAATGCTTGCTACTCATCTTGAGGAGGTGGGCTCTTACTACTGCAGGTTGTCTGACAGAGACAA
TGCTGAGCTCAGCATAGGTCATGGTGACACTGGAAAAAAAGGGGGTACTGAGCCTGGCAAATATACCAAC
TACCAGTCCTCCTTTATCTCCTTTCTCCCTGGTTTCTTGCAAATCTCGATGTGGCAGTATATATATAGCAGC
TGAGCCCTCTTGCTTTGTGAGTCTTTTTCCCCCCATTTGTGAGATGAATGTTAATAGTTTGGTTTCTTGGAT
GTCACATTACCTTTGTAAGGGGTTAGGGCTTTGGTTGTATTATTGGGTTGCATGTTTTCATTGTTTTGGACG
TTTTTTTTTCTGGTGGGGGACGGGTTCAGGGGGGTTGAAATCCAAGCTTGACAGATGACTTTTTTTTTCCC
TCCATCAATACACCTAAGCAATAGACAAGTTTGAAGTGAATTGCCTGCTTCGAGGGCAAAATATTCCTTCA
GTCAGGGGAGAAACCCAGAACAATGAAAGGTGTACCTACTTGGAAAGGTCCATGTGCTATTCAGGGACC
CATTTGGGAATCTTTCCACAATTATTCCATTAAGAGGTGTTGCTGCATTCATTGGTCGGGGAGGGGATGAA
ACACCTGAAAGGAGAAAAAGGATTCTGTGATCAAATGGAAATGAAAGGGAAGCAGAGCTAATAGCTTGCT
AAATAACTGGGTTTTTTCGACAATCCCTCCCCCTTTTAGACCCCAGCTTATTTCTTATGGATGCCGTATAGC
GGCACCAGCTTGATGGGGAGAGGGTTTGATGAATAGCACAAAGGCACTGGGTATTCCCTGGAGGCTGTC
CCTTTAAAAGAGAATCCTAGTTTATTCTGGGGGAGGGGATACACATATTAGAGCAGGCAAAAAAGGACAAG
GAATAAAAGTAATTCACCCCCTTCCTAGCCATTGTATTGAGATGCAAAGGCTGCTTCCTACAGGAGGGTGC
TAACCTTGGCTAGCTCCCTCTGTTTCTCTTTGAGGGAATTTAGTCAGGCTATGGATTCATTTACAACTGTTA
GTCATGTGGCCATGTGTGAAGGAGCAGATGCCAGTTTTAATGTATTTTGCCCGAAGTTACAATTTGATAGG
AGCCACTGTCAGGAAGCTCCAGGTTTTTAAGCTATTTCAACACGCCCTCCCCAAATTGGAACAGTGCCAAA
AGTGCCACCCTTTCTATCTCTTCCTCCTATCCCCCTCCCCACCATTCAGTCCTCAGCCTACTGCCCAGCCC
CCTCCTTCTTCTCTATTAAGATCAATATTCCTGCAGGTCAGGGACAAGCAGCAGATGGGTCACAGGCTTTT
TTCAACCAGTTCTTTTCACAGGCAGCAGATTGCAGCTCTGGATCTGGCTAATATTT

Figure S8. Evolutionary conserved regions for *Plxna2* and *Dcx* used in luciferase constructs

A ECR of *Plxna2*; Chr1: 194,607,138-194,608,136
B Promotor region of *Dcx*; ChrX: 143,931,400-143,933,590
The letters written in red indicate putative Sox11 binding sites, the letters written in blue indicate E-Boxes (putative TCF4 binding sites). Highligthed in yellow are the sites of the oligonucleotides used in EMSAs.

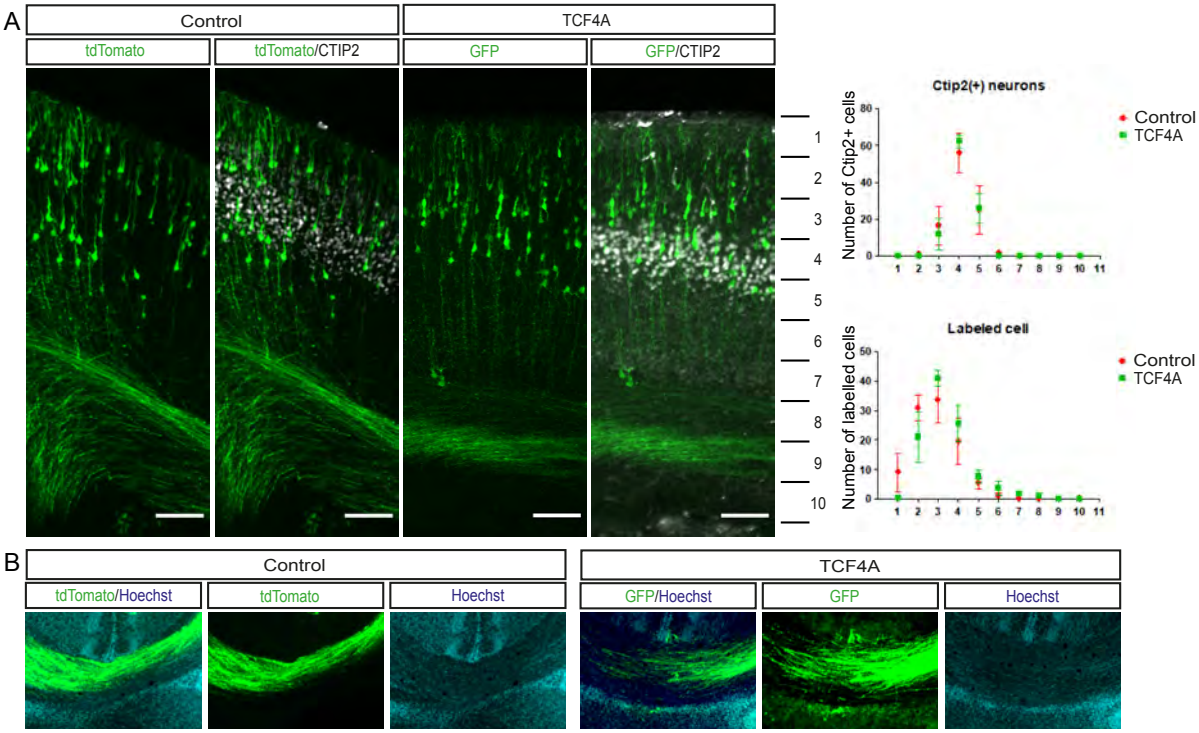

Figure S9. Analysis of TCF4A overexpression by *in utero* electroporation and the binding of TCF4A

A Expression constructs were introduced into E13.5 wild-type brains through *in utero* electroporation. Brains were dissected out at P0.5 for analyses. Cells that had taken up the expression construct are detected by the expression of the fluorescent reporter (coloured in green). Quantification of control pCAG-tdTomato vector and pCAG-TCF4A-IRES-GFP vector electroporated cells and expression of CTIP2 (grey) in the cortical plate. No difference in the number of CTIP2+ cells or the distribution of labelled cells was observed. n = 3, scale bar = 100 µm
B Expression vectors were *in utero* electroporated into E14.5 wild-type brains. Brains were dissected out at for analyses. Electroporated cells are shown in green. Note that processes of TCF4A overexpressing neurons are able to cross the midline. n = 3, scale bar = 100 µm

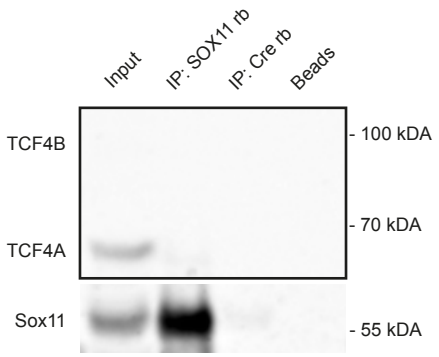

Figure S10. Analysis of TCF4A binding to SOX11 using TCF4KO protein lysates

Co-immunoprecipitation assay conducted with E18.5 cortex lysates from *Tcf4*KO mice using anti-SOX11 antibody. Upper panel: detection with anti-TCF4 antibody. Lower panel: detection with anti-SOX11 antibody. The blots presented are cropped. TCF4B was co-immunoprecipitated with SOX11, but not with an isotype control for IgG and Agarose A Beads alone. The interaction was confirmed in three independent biological replicates (n = 3); rb = antibody raised in rabbit.

Table S1. Differential expressed genes in the *Satb2* cluster and GO term analysis. Related to Figure 3.

Click here to Download Table S1

Table S2. Differential expressed genes in the limited *Satb2* cluster and GO term analysis. Related to Figure 3.

Click here to Download Table S2

Table S3. Differential expressed genes in the upper layer cluster and GO term analysis. Related to Supplemental Figure 3.

Click here to Download Table S3

Table S4. Differential expressed genes in the deep layer cluster and GO term analysis. Related to Supplemental Figure 4.

Click here to Download Table S4

Table S5. Differential active regulons in the *Satb2*, the limited Satb2, the deep layer and the upper cluster. Related to Figure 3 and Supplemental Figure 3 and 4.

Click here to Download Table S5

Table S6. Overlap of differential expressed genes and the predicted Sox11 regulon in the *Satb2* cluster and GO term analysis. Related to Figure 5.

Click here to Download Table S6